

**ANALYZING SORPTION EXCLUSION EFFECTS FOR THE  
CO<sub>2</sub>/CH<sub>4</sub> GAS PAIR USING MATRIMID® CMS DENSE FILMS**

A Thesis  
Presented to  
The Academic Faculty

by

Taylor C. Vessel

In Partial Fulfillment  
of the Requirements for the Degree  
Master of Science in Chemical Engineering in the  
School of Chemical & Biomolecular Engineering

Georgia Institute of Technology  
August 2023

Copyright © 2023 by Taylor C. Vessel

**ANALYZING SORPTION EXCLUSION EFFECTS FOR THE  
CO<sub>2</sub>/CH<sub>4</sub> GAS PAIR USING MATRIMID® CMS DENSE FILMS**

Approved by:

Dr. William J. Koros, Advisor  
School of Chemical & Biomolecular Engineering  
*Georgia Institute of Technology*

Dr. Ronald W. Rousseau, Professor Emeritus  
School of Chemical & Biomolecular Engineering  
*Georgia Institute of Technology*

Dr. Ryan P. Lively, Professor  
School of Chemical & Biomolecular Engineering  
*Georgia Institute of Technology*

Date Approved: July 24, 2023

To my dad, without him I would have never considered the field of chemical engineering.

## ACKNOWLEDGEMENTS

It is an incredible honor to have studied at the Georgia Institute of Technology under the leadership and guidance of Dr. Koros. I have met so many amazing people here, and I will miss my time I spent in Atlanta at this outstanding institute. I truly cherished being able to work with and learn from so many brilliant people during my time here.

I would like to sincerely thank my committee members: Dr. Ronald W. Rousseau and Dr. Ryan P. Lively. Although I never attended Louisiana State University, I was raised an LSU Tiger fan, and Dr. Rousseau and I connected over this. I had the privilege of taking Dr. Lively's mass transfer course which was extremely enriching to my understanding and growth as a chemical engineer. I greatly appreciated his teaching style and his willingness to help in time of struggle or misunderstanding of concepts.

I also would like to thank Dr. Martha Grover and Mrs. Janice Whatley for their support and guidance from the minute I arrived on campus. Thank you both for helping me navigate through graduate school at Georgia Tech.

I would like to also thank all my chemical engineering professors back at West Point. Dr. Nagelli, Dr. Armstrong, and MAJ Chin – thank you for encouraging me to pursue graduate level chemical engineering.

I also would like to thank the National GEM Consortium. I would not have pursued graduate education without their support, both financially, professionally, and emotionally. It has been an honor to be a GEM Fellow.

I would like to thank all the members of the Koros group, past and present. It is an honor to be able to be in the group in the first place. It made research a little easier being able to stand on the shoulders of giants.

I would also like to specifically thank Dr. Zhongyun Liu, a member of the Koros group. He went out of his way to welcome me into the group and made me feel valued and appreciated. He taught me just about every experimental technique needed to be successful working with CMS and for that I will always be grateful.

I would also like to make a special thank you to both Dr. Zachary Campbell and Asia Taylor, two incredible members of the Koros group that contributed to this body of work with Scanning Electron Microscopy (SEM) imaging and countless hours of sorption module calibration and appendix preparation, respectively.

I also would like to thank Dr. Koros. He took a chance on me, and despite hardship throughout my time at Georgia Tech, he always supported me. He is one of the kindest professors I have ever met, and exactly the way I will strive to be as leader in the future. Even after our focuses for my research changed, he always smiled (through his mask) and pushed me to continue, regardless of how frustrating or difficult research got. I learned so much from him, and I hope that I can represent him and his group strongly and positively beyond Georgia Tech. Thanks again, Dr. Koros.

I would like to thank my family for their undying support. My parents, William and Rebecca Vessel have been the most unwavering support system throughout all my time in school. I would not have completed this without them. I would also like to thank my little brother, Landon. Thank you for being there for me.

And finally, I would like to thank my best friend, my wife, Gaby. I can't wait to see where life takes us, and I'm so thankful that you have been by my side every step of the way.

# TABLE OF CONTENTS

<b>ACKNOWLEDGEMENTS</b>	<b>iv</b>
<b>LIST OF TABLES</b>	<b>ix</b>
<b>LIST OF FIGURES</b>	<b>xi</b>
<b>SUMMARY</b>	<b>xiv</b>
<b>CHAPTER 1. Introduction</b>	<b>1</b>
1.1 Personal Motivation	3
1.2 Membrane-Based Gas Separation	4
1.3 Thesis Structure	6
1.4 References	7
<b>CHAPTER 2. THEORY AND BACKGROUND</b>	<b>9</b>
2.1 Overview	9
2.2 Discussion	10
2.3 References	19
<b>CHAPTER 3. MATERIALS AND EXPERIMENTAL METHODS</b>	<b>21</b>
3.1 Formation of CMS Membranes	21
3.1.1 Precursor Film Formation	21
3.2 Pyrolysis Equipment and Protocol	22
3.2.1 Protocols	23
3.2.2 Additional comments on pyrolysis protocols	26
3.3 Sorption Methodology	27
3.4 References	31
<b>CHAPTER 4. CHARACTERIZATION OF MATRIMID® CMS</b>	<b>32</b>
4.1 Overview	32
4.2 Traditional Pore Size Characterization Using CO <sub>2</sub> Physisorption	32
4.3 Morphology Characterization Using WAXD and RAMAN Spectroscopy	34
4.4 Matrimid® CMS Dense Film Scanning Electron Microscopy Imaging	35
4.5 Characterization of Matrimid® CMS Dense Films using XPS	36
4.6 References	38
<b>CHAPTER 5. CO<sub>2</sub>/CH<sub>4</sub> SORPTION IN MATRIMID®-DERIVED CMS</b>	<b>39</b>
5.1 Introduction	39
5.2 CO <sub>2</sub> Sorption Results	40
5.3 CH <sub>4</sub> Sorption Results	44
5.4 Dual Mode Parameters	48
5.5 Discussion	54
5.6 References	57

<b>CHAPTER 6. CONCLUSIONS AND RECOMMENDATIONS</b>	<b>58</b>
<b>6.1 Conclusions</b>	<b>58</b>
<b>6.2 Recommendations</b>	<b>59</b>
<b>6.3 References</b>	<b>60</b>
<b>APPENDIX A. COMPARISON TO PREVIOUS WORK</b>	<b>61</b>
<b>APPENDIX B. ADDITIONAL SORPTION EXPERIMENT DATA</b>	<b>64</b>

## LIST OF TABLES

Table 1 – CMS-550 Pyrolysis Protocol	24
Table 2 – CMS-700 Pyrolysis Protocol	24
Table 3 – CMS-900 Pyrolysis Protocol	25
Table 4 – Burnout Protocol	26
Table 5 – Dual-mode sorption parameters for CO <sub>2</sub> & CH <sub>4</sub> Matrimid® CMS-550 dense film membranes	49
Table 6 – Dual-mode sorption parameters for CO <sub>2</sub> & CH <sub>4</sub> Matrimid® CMS-700 dense film membranes	49
Table 7 – Dual-mode sorption parameters for CO <sub>2</sub> & CH <sub>4</sub> Matrimid® CMS-900 dense film membranes	50
Table 8 – Matrimid® CMS-550 CH <sub>4</sub> Test Data	65
Table 9 – Matrimid® CMS-550 CO <sub>2</sub> Test Data	65
Table 10 – Matrimid® CMS-550 CH <sub>4</sub> Test Data	66
Table 11 – Matrimid® CMS-550 CO <sub>2</sub> Test Data	66
Table 12 – Matrimid® CMS-700 CH <sub>4</sub> Test Data	67
Table 13 – Matrimid® CMS-700 CO <sub>2</sub> Test Data	67

Table 14 – Matrimid® CMS-900 CH<sub>4</sub> Test Data 68

Table 15 – Matrimid® CMS-900 CO<sub>2</sub> Test Data 68

## LIST OF FIGURES

Figure 1 – Schematic representation of a CMS asymmetric hollow fiber production process	2
Scheme 1 – Matrimid® Polyimide, Huntsman Chemicals	3
Figure 2 – CMS derived from Matrimid®, showing effects of pyrolysis temperature on CO <sub>2</sub> /CH <sub>4</sub> separation performance compared to the 2008 polymer upper bound	10
Figure 3 – Background for transient (time lag) experiment to estimate $D_A = l^2 / (6\theta)$ determination	12
Figure 4a – Constituent contributions to CMS-derived from Matrimid® showing effects of pyrolysis permeability, diffusion, and sorption properties	12
Figure 4b – Mixed Matrix Morphology	12
Figure 5 – Hypothetical vision showing self-consistent basis for developing CO <sub>2</sub> /CH <sub>4</sub> sorption selectivity and diffusion selectivity with increasing pyrolysis temperatures	15
Figure 6 – Placement of flat, polymeric precursor films on a quartz plate for pyrolysis	22
Figure 7 – Schematic of pyrolysis furnace and its setup	23
Figure 8 – Schematic of pressure decay sorption system that was used throughout the entirety of this work	28

Figures 9a, b, c, d, e – $dV/d\log W$ (differential pore volume) vs. pore size ( $W$ ) for CMS Membranes pyrolyzed at (a) 750°C, (b) 800°C, (c) 850°C, (d) 875°C, (e) 900°C	33
Figures 10a, b – (a) Wide-angle X-ray diffraction (WAXD) and (b) Raman spectroscopy results for Matrimid®-derived CMS pyrolyzed under inert Argon from 750 –900°C	34
Figure 11 – SEM Imaging of Matrimid® CMS-550 edge and surface, respectively	35
Figure 12 – Atomic Composition Results from XPS in Matrimid® CMS-550, 700, and 900°C	37
Figure 13a – CMS-550 CO <sub>2</sub> Sorption Results at 35 °C	40
Figure 13b – CMS-700 CO <sub>2</sub> Sorption Results at 35 °C	41
Figure 13c – CMS-900 CO <sub>2</sub> Sorption Results at 35 °C	42
Figure 13d – Summary CO <sub>2</sub> Sorption Results for CMS-550, 700, and 900 at 35 °C	43
Figure 14a – CMS-550 CH <sub>4</sub> Sorption Results at 35 °C	44
Figure 14b – CMS-700 CH <sub>4</sub> Sorption Results at 35 °C	45
Figure 14c – CMS-900 CH <sub>4</sub> Sorption Results at 35 °C	46
Figure 14d – Summary CH <sub>4</sub> Sorption Results for CMS-550, 700, and 900 at 35 °C	47
Figure 15a – $S_{CO_2} = C_{CO_2}/p_{CO_2}$ and $S_{CH_4} = C_{CH_4}/p_{CH_4}$ at 100 psia vs. $T_{pyrolysis}$ at 550, 700 and 900 °C	48
Figure 15b – $\alpha_S = S_{CO_2}/S_{CH_4}$ vs. $T_{pyrolysis}$ at 550, 700 and 900 °C	49

Figure 16a – $C_H'$ versus $T_{\text{pyrolysis}}$ at 550, 700 and 900 °C	50
Figure 16b – $b$ (affinity constant) versus $T_{\text{pyrolysis}}$ at 550, 700 and 900 °C	51
Figure 16c – $k_{c,i}$ versus $T_{\text{pyrolysis}}$ at 550, 700 and 900 °C	52
Figure 16d – $K$ versus $T_{\text{pyrolysis}}$ at 550, 700 and 900 °C	53
Figure 17 – Kiyono CO <sub>2</sub> & CH <sub>4</sub> Sorption isotherms for Matrimid® CMS-550 membranes prepared with 1 ppm O <sub>2</sub> /Ar inert pyrolysis	62
Figure 18a – Vessel CO <sub>2</sub> Sorption Dual Mode Model fit for Matrimid® CMS-550	62
Figure 18b – Vessel CH <sub>4</sub> Sorption Dual Mode Model fit for Matrimid® CMS-550	63

## SUMMARY

This thesis uses the so-called dual-mode sorption model to analyze Matrimid® polyimide-derived carbon molecular (CMS) thin films. This model provides a useful framework to analyze and understand sorption in complex CMS morphology. The model is also helpful to connect morphology to the pyrolysis process used to create it. The dual mode model includes coexisting continuous and dispersed Langmuir terms. The model parameters related to these environments are reported and discussed in this work.

CMS based membranes have been applied towards many different gas-pair separations. CMS thin films have appealing separation performance for key gas pairs; the carbon dioxide/methane pair, which is practically important, is the focus of this study. Previous measurements on CMS film sorption for this pair have been done. Surprisingly, applying the dual-mode sorption model to such thin films created from Matrimid® *over a range of pyrolysis temperatures* has not been done previously and is considered here. This thesis characterizes sorption properties of such CMS thin films for the CO<sub>2</sub>/CH<sub>4</sub> pair and adds insights relevant to their separation. Suggestions for the next steps to extend this study are also provided.

## CHAPTER 1. INTRODUCTION

Over the last several decades, under Department of Energy BES support, the Koros group has developed a new generation of membranes based on carbon molecular sieve (CMS) membranes to assist in achieving sustainability in globally important separations (1-4). These materials are moving forward toward commercialization. The current exciting time is similar to that in the late 1970's when glassy polymers were shown to have unusually desirable properties relative to rubbery polymers (5-6). Specifically, at that time, glassy polymer asymmetric hollow fibers enabled formation of ultrahigh surface to volume membranes with up to 10,000 m<sup>2</sup> per cubic meter of module volume. Moreover, such glassy polymer membrane gave unusually high selectivities for gas pairs such as CO<sub>2</sub> and CH<sub>4</sub>, O<sub>2</sub> and N<sub>2</sub>, and H<sub>2</sub> and CH<sub>4</sub> for moderate feed conditions. One class of such glassy polymers, the polyimides, emerged as the most attractive. Due to appeal of CH<sub>4</sub> as a low carbon fuel, markets expanded, and increasingly high CO<sub>2</sub>-containing resources were pursued due to limited availability of low CO<sub>2</sub> natural gas resources. To avoid emitting the high levels of CO<sub>2</sub> extracted from the natural gas, reinjection to the source well became increasingly necessary. Moreover, the ability to avoid using toxic amine absorption fluids made membranes increasingly appealing as offshore installations were pursued (2). The high-pressure natural gas feeds from such well, however, were often supercritical fluids that swelled even highly rigid glassy polymers, causing them to be "plasticized", thereby undermining their highly selective natures. It was discovered that crosslinking such materials after spinning into asymmetric forms moderated loss in their size and shape selectivities under highly aggressive natural gas feeds. While this crosslinking approach

is viable, it reduces intrinsic membrane productivity (permeability), thereby requiring increasingly larger and more expensive offshore processing facilities to remove the CO<sub>2</sub> (7). The period in the 1980's-1990's coincided with the discovery of mega fields in the deep water off-shore—often many miles from on-shore processing where fixed platforms are extremely expensive. The increasing CO<sub>2</sub> contents also challenged the ability of even crosslinked membranes to deliver adequate selectivity-productivity tradeoff properties. Zeolite and ceramic membrane materials can deliver the required selectivity and productivity to purify such challenging feeds, but at a cost of roughly *100 times more than crosslinked polymers in modular form*. On the other hand, CMS membranes are estimated to offer similar selectivity values to zeolites with much less brittle properties that may cost only 3 times more than glassy polymers in asymmetric forms (8). Discoveries that asymmetric polyimide membranes could be pyrolyzed as shown in Figure 1 with good mechanical properties and no plasticization even at 1500 pounds per square inch atmosphere of CO<sub>2</sub> rich streams made CMS membranes change agents for such challenging separations (2).

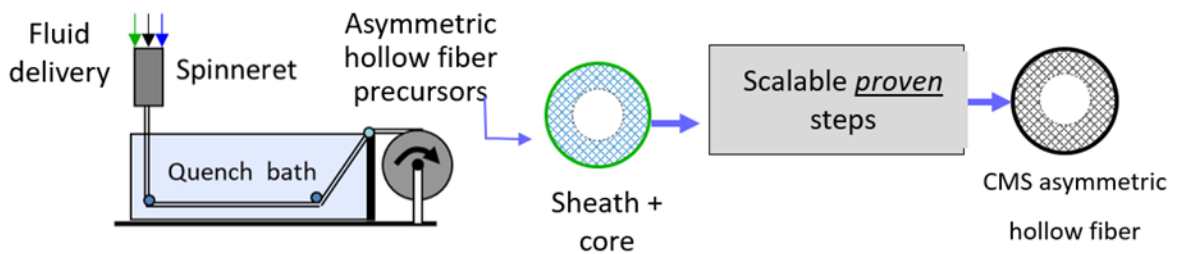
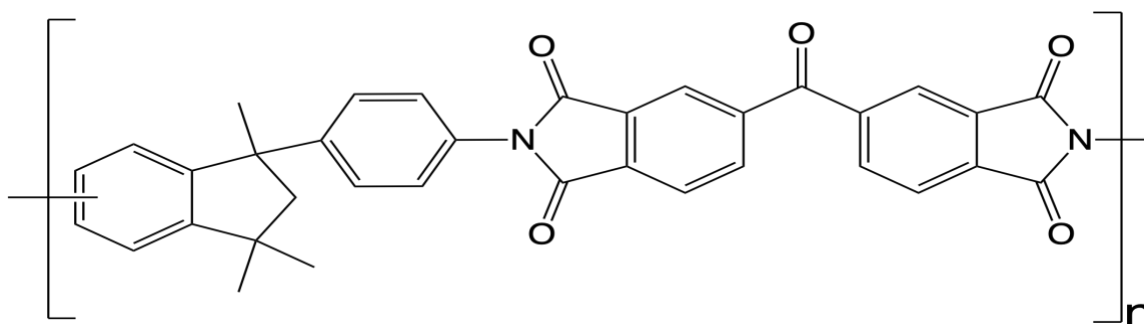


**Figure 1: Schematic representation of a CMS asymmetric hollow fiber production process**

A recent fundamental discovery suggests that not only molecular sieving *diffusion selectivity*, but also *thermodynamic exclusion selectivity* can be tuned in CMS membranes (5), and this is the topic of the current thesis. Such a combination of factors enables a new

set of options to promote sustainable separations that are not available to polymers or non-carbon inorganic membranes (6-10).

This thesis begins the process of understanding and explaining the fundamental properties for the exclusion selectivity related for CMS membranes derived from a particular commercially available precursor, Matrimid®, shown in Scheme 1. A PhD student in the Koros group, Nicholas Leon, is pursuing the fundamental topic of *molecular sieving diffusion selectivity* for Matrimid®-derived CMS that complements the exclusion selectivity topic. Understanding and controlling these two complementary sorption and diffusion factors will allow creating a new generation of membranes, which will have applications even beyond natural gas.



**Scheme 1: Matrimid® Polyimide, Huntsman Chemicals (11)**

## 1.1 Personal Motivation

There has previously been work done on CMS thin films but providing insight into the structure (in the Continuous and Langmuir phases) of these membranes is my motivation in this thesis. Utilizing the dual mode model to understand the structure of CMS thin films has been the driving force behind this research, ultimately aiding in determining their behavior during sorption and testing.

## 1.2 Membrane-Based Gas Separation

Membrane separation is an emerging technology, and it has been suggested that membrane technology may provide attractive alternative to traditional thermally driven methods for gas separation because of lower capital and operating costs. Currently, insufficient selectivity, a narrow range of useful operation conditions, and high manufacturing costs limit the application of membranes to replace thermally driven separations. Nevertheless, several studies have shown that a combination of membranes and conventional absorption or distillation units can provide better separation performance with attractive energy and economic savings. Conventional polymeric membranes have been well studied for gas separations. Polymer membranes have good mechanical and chemical properties and are currently implemented in industry for gas separation application. In 1991, Robeson reported that the performances of solution processable polymers are limited by a trade-off relationship (commonly referred to as the polymer upper bound) between productivity (permeability) and separation efficiency (selectivity) for common gas pairs (12). This fact is usually referred to as the “polymer upper bound” and summarizes productivity (permeability) and separation efficiency (selectivity) for important gas pairs.

Carbon molecular sieve (CMS) membranes are a type of synthetic membrane material that consists of highly porous carbon structures. These membranes are primarily designed to separate gases based on their molecular size and shape, making them useful for various applications such as gas separation, purification, and filtration processes. CMS membranes have a unique structure with a network of micropores and mesopores. The carbon material used in the membrane is typically derived from organic polymers,

such as polyimide or cellulosic, which are carbonized to create the porous structure. The pores in CMS membranes are typically in the range of 0.3 to 0.8 nanometers. The separation mechanism of CMS membranes is based on the selective adsorption and diffusion of gas molecules. Smaller molecules can enter and diffuse through the micropores more easily than larger molecules, leading to separation. This molecular sieving effect allows for the separation and purification of gases. CMS membranes can find applications in various gas separation processes, including the separation of air into oxygen and nitrogen, the removal of carbon dioxide (CO<sub>2</sub>) from natural gas or biogas and hydrogen purification. These membranes ideally offer high selectivity and permeability for specific gas pairs, making them valuable for industrial processes. Carbon molecular sieve membranes offer several advantages over other types of gas separation techniques. They provide high selectivity, high permeability, and good stability, making them suitable for continuous and large-scale separation processes. CMS membranes can be fabricated as thin films or hollow fibers, allowing for integration into different membrane module configurations. This work will be focused on thin dense films to allow fundamental property determinations.

While CMS membranes have demonstrated significant potential, there are some limitations to consider. The fabrication process can be complex and requires precise control over the carbonization and activation steps to achieve the desired pore structure. The performance of CMS membranes can also be affected by factors such as temperature, pressure, and the presence of impurities in the gas streams. The main challenge lies in the process to form these novel materials. These procedures are often tedious and extremely painstaking in that the researcher or preparer must be very meticulous in every

single step. Researchers are continuously working on improving the performance and scalability of carbon molecular sieve membranes. This includes exploring different carbon precursors, optimizing membrane fabrication techniques, and developing novel membrane structures to enhance selectivity and permeability. In summary, carbon molecular sieve membranes are advanced materials that can selectively separate gases based on their molecular size and shape. These membranes have potential applications in various industries and are subject to ongoing research and development to improve their performance and broaden their range of applications.

### **1.3 Thesis Structure**

This thesis will provide background into CMS thin film membranes and mention previously done work with them to lay the foundation of the current state of research on them. Next discussion of relevant sorption experiments and results conducted by the author will be provided to explain the structure of these films. The dual mode model of CMS morphology is introduced to understand directly measured sorption isotherms at varying pressures for three different pyrolysis temperatures. Results for such directly measured sorption values are compared to indirect measurement of sorption results at a particular feed pressure (100 psia). Extension of the discussions that allows interpretation of trends in both the sorption properties and model parameters. Prior complementary characterization of CMS materials is considered. In addition, new X-ray photoelectron spectroscopy (XPS) characterization is considered to add additional insights into the CMS properties and model parameters. Finally, discussion of all the results will be done to suggest steps forward to further the insight into this field.

## 1.4 References

1. Liu, ZY; Qiu, WL; Quan, WY; Koros, WJ, Advanced carbon molecular sieve membranes derived from molecularly engineered cross-linkable copolyimide for gas separations-) NATURE MATERIALS, 22 (1), 109-116 (2023).
2. Koros, WJ; Zhang, C, Materials for next-generation molecularly selective synthetic membranes, Nature Materials, 16, 289-297 (2017).
3. Hays, SS; Sanyal; Leon, NE; Arab, P; Koros, WJ, Envisioned role of slit bypass pores in physical aging of carbon molecular sieve membranes, CARBON,157,385-394 (2020).
4. Sanyal, O; Zhang, C; Wenz, GB; Fu, SL; Bhuvania, N; Xu, LR; Rungta, M; Koros, Next generation membranes using tailored carbon, CARBON, 127 688-698 (2018).
5. Zhang, C; Koros, WJ, Ultraselective Carbon Molecular Sieve Membranes with Tailored Synergistic Sorption Selective Properties, ADVANCED MATERIALS, 29 (33), Article Number: 1701631(2017).
6. National Academies of Sciences, Engineering, and Medicine 2019. A Research Agenda for Transforming Separation Science. Washington, DC: The National Academies Press <https://doi.org/10.17226/25421>.
7. <https://www.offshore-technology.com/projects/libra-oil-field-santos-basin/>
8. Koros, W. J.; Lively, R. P., Water and beyond: Expanding the spectrum of large-scale energy efficient separation processes. Aiche Journal 2012, 58 (9), 2624-2633.

9. Sholl, DS; Lively, RP, Seven chemical separations to change the world. *Nature* 532, 435–437 (2016).
10. Oak Ridge National Laboratory. *Materials for Separation Technologies: Energy and Emission Reduction Opportunities* (2005).
11. Leon, NE, Matrimid® Polyimide, Huntsman Chemicals, ChemDraw Figure (2023).
12. Lloyd M. Robeson, Correlation of separation factor versus permeability for polymeric membranes, *Journal of Membrane Science*, Volume 62, Issue 2, 1991, Pages 165-185, 0376-7388, [https://doi.org/10.1016/0376-7388\(91\)80060-J](https://doi.org/10.1016/0376-7388(91)80060-J).

## CHAPTER 2. THEORY AND BACKGROUND

### 2.1 Overview

Although this thesis primarily focuses on the topic of exclusion selectivity for CMS membranes, establishing a general framework related the membrane paradigm provides a perspective for the reader to understand the basis for of work. Molecularly selective membranes rely upon sorption and diffusion contributions of a penetrant A, reflected by a sorption coefficient ( $S_A$ ) and a diffusion coefficient ( $D_A$ ). The permeability ( $P_A$ ) of A in Equation 1 characterizes fundamental materials productivity in Barrers ( $1 \text{ Barrer} = 10^{-10} \text{ cc (STP)} \cdot \text{cm} \cdot \text{cm}^{-2} \cdot \text{s}^{-1} \cdot \text{cm Hg}^{-1}$ ). Functionally,  $P_A$  equals the normalized flux,  $N_A$ , of penetrant A across a membrane with a selective layer,  $l$ , due to a partial pressure,  $\Delta p_A$  (or fugacity,  $\Delta f_A$ ), difference between upstream and downstream faces. The permselectivity,  $\alpha_{AB}$ , equals the ratio of permeabilities of component A vs. B, and can be factored into effective (average) diffusion selectivity,  $\alpha_{D,AB}$  and sorption selectivity,  $\alpha_{S,AB}$ , terms, viz.,

$$P_A = \frac{N_A \cdot l}{\Delta f_A} = D_A S_A \quad (1)$$

$$\alpha_{AB} = \frac{P_A}{P_B} = \frac{D_A S_A}{D_B S_B} = (\alpha_{D,AB})(\alpha_{S,AB}) \quad (2)$$

## 2.2 Discussion

The CMS results in Figure 2 show a revolutionary  $\text{CO}_2/\text{CH}_4$  selectivity over 3500 for the 900°C pyrolyzed Matrimid® sample in Figure 2 (1). Dramatic increases in both diffusion selectivity  $\alpha_{D,AB}$  and sorption selectivity  $\alpha_{S,AB}$  have been reported as pyrolysis temperature increases (1), indicating that pyrolysis temperature is a powerful multifaceted tool. Understanding exactly why and how this tool functions will allow creating advanced

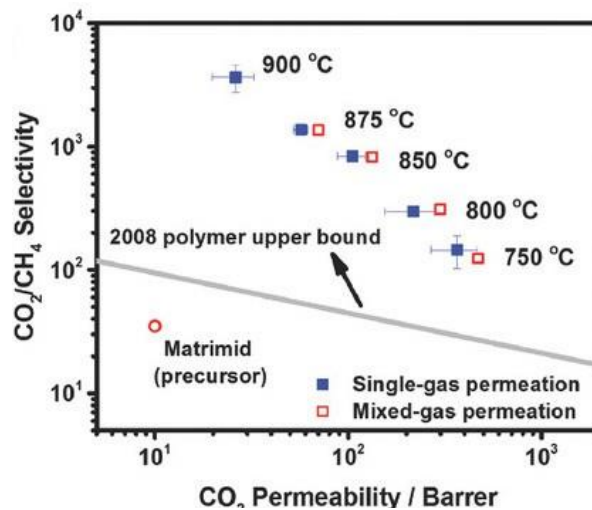


**Figure 0: CMS derived from Matrimid®, showing effects of pyrolysis temperature on  $\text{CO}_2/\text{CH}_4$  separation performance compared to the 2008 polymer upper bound (1).**

membranes based on the CMS platform, and this thesis begins this process by focusing on the sorption terms in Equation 1 and 2.

The 900 °C mixed gas results were not reported in Figure 2 since the selectivity was so high that it was difficult to measure accurately due to ultrahigh selectivity ~ 3500 for these membranes.

The effective diffusion coefficient is, of course, a kinetic factor while the effective sorption coefficient is thermodynamic in nature; nevertheless, both fundamental coefficients can be tuned by *molecular engineering* (2). Zhang’s paper (1) identified the above trend involving “ultraselectivity” in 2017 (1) and used an approach based on Equations 1 and 2 to estimate the constituent contributions to the revolutionary separation performance. He fixed the feed pressure at 100 psia with a vacuum permeate downstream and applied traditional membrane approaches to estimate the diffusion and sorption contributions to the permselectivity. For the reader’s convenience a short summary of the approach used to generate Figure 3 is provided regarding effective P, D, S values vs. pyrolysis temperature. The approach, used to evaluate variables in Figure 2 at each of the pyrolysis temperatures for the pure gas case still starts with Equation 1 with for A= CO<sub>2</sub> and B= CH<sub>4</sub>. The effective D<sub>A</sub> and S<sub>A</sub> coefficients can be estimated in various ways (2), including direct measurements of P<sub>A</sub> in Equation (1) with direct measurement of S<sub>A</sub> = C<sub>A</sub> /p<sub>A</sub> where C<sub>A</sub> is measured for a given p<sub>A</sub> followed by calculation of D<sub>A</sub> = P<sub>A</sub> /S<sub>A</sub>. This approach requires two separate experiments; however, Zhang used an alternate approach in which the transient time lag (θ), illustrated in Figure 3 was used. The Q(t)=N<sub>A</sub>(t)· [Membrane area] in Equation (1), and D<sub>A</sub> = l<sup>2</sup>/(6θ) to evaluate D<sub>A</sub>, the “average” or “effective” diffusion coefficient (2). The D<sub>A</sub> is an average value from the upstream to the downstream, shown in Equation (1 and 2). With the downstream at vacuum, as it in Zhang’s work, the downstream sorbed concentration is effectively zero, and S<sub>A</sub> =P<sub>A</sub> / D<sub>A</sub> with D<sub>eff</sub> =D<sub>A</sub> shown in Equation (3). The combined time lag and steady state permeation approach in Figure 3 allows rapid identification of materials for further study detailed studies, as Zhang did in his study (1).

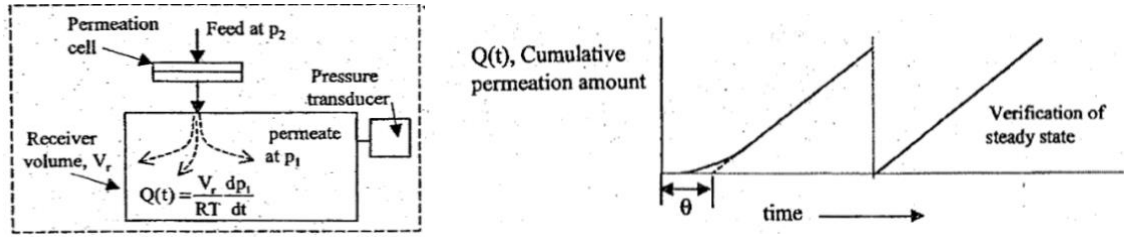


Figure 3: Background for transient (time lag) experiment to estimate  $D_A = l^2 / (6\theta)$  determination (2)

$$D_{\text{eff}} = \frac{\int_0^{c_2} (D \cdot dC)}{\int_0^{c_2} (dC)} = \int_0^{c_2} \frac{D \cdot dC}{C_2} = D_A \quad (3)$$

Zhang evaluated  $P_A, P_B,$  and  $D_A, D_B, S_A,$  and  $S_B$  shown below in Figure 4a, illustrating interesting trends in all the parameters vs. pyrolysis temperature (5). Zhang's suggested a "mixed matrix" morphology in Figure 4b, consistent with the trends seen in Figure 4a-iii.

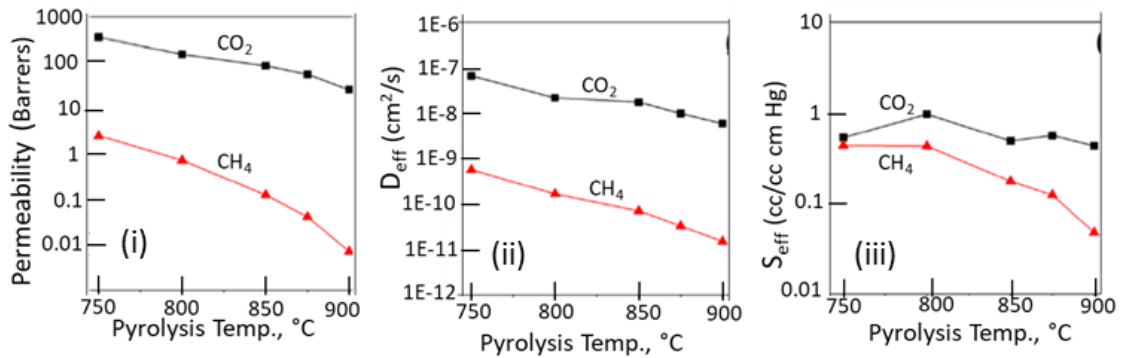


Figure 4a: Constituent contributions to CMS-derived from Matrimid® showing effects of pyrolysis permeability, diffusion, and sorption properties (5)

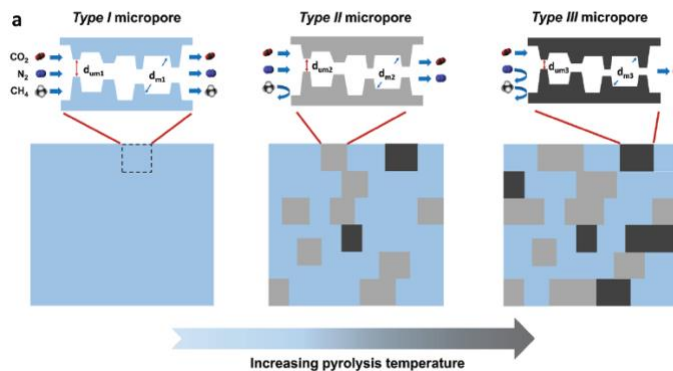


Figure 4b: Mixed Matrix Morphology (5)

However, it does not provide such a self-consistent connection to a mechanism to create such a complex proposed mixed matrix patchwork. This thesis takes a first step toward providing such a self-consistent integrated vision of how and why CMS morphologies may evolve to explain the effective sorption parameters in Figures 4a-iii.

Conventional molecular sieves like zeolites or MOFs show sorption isotherms that are described adequately by Langmuir isotherms (3-4), but careful sorption measurements for both CO<sub>2</sub> and CH<sub>4</sub> in CMS showed consistent deviation from the simple Langmuir form (5). Fortunately, combined Langmuir and Henry's law sorption terms, in the so-called "dual mode" mathematical formalism, fit the CMS results well. Moreover, the terms and model parameters have physical meaning, with the Henry's term is associated with a low (5,6) volume fraction of a rigid disordered continuous ("C") in addition to distributed microporous Langmuir domains ("L") as shown in Equation 4.

$$C_i = C_{C,i} + C_{L,i} = k_{C,i}f_i + \frac{C'_{L,i}b_i f_i}{1 + b_i f_i} \quad (4)$$

Here,  $k_{C,i}$  is the continuous mode Henry's law sorption constant of component  $i$ ;  $C'_{L,i}$  is the Langmuir sorption capacity;  $b_i$  is the Langmuir affinity constant, and  $f_i$  is the local fugacity of while  $K_i = \frac{C'_{L,i}b_i}{k_{C,i}}$ . Also, mixed gas permeability expressions for a binary A and B feed are given in Equations 5a and b, with subscripts 2 and 1 referring to upstream and downstream, respectively.

$$P_A = D_{CA}k_{CA} \left[ 1 + \frac{F_A K_A f_{A2}/(f_{A2} - f_{A1})}{1 + b_A f_{A2} + b_B f_{B2}} - \frac{F_A K_A f_{A1}/(f_{A2} - f_{A1})}{1 + b_A f_{A1} + b_B f_{B1}} \right] \quad (5a)$$

$$P_B = D_{CB}k_{CB} \left[ 1 + \frac{F_B K_B f_{B2}/(f_{B2} - f_{B1})}{1 + b_A f_{A2} + b_B f_{B2}} - \frac{F_B K_B f_{B1}/(f_{B2} - f_{B1})}{1 + b_A f_{A1} + b_B f_{B1}} \right] \quad (5b)$$

The parameters,  $F_i = D_{Li} / D_{Ci}$ , characterize the ratio of diffusion coefficients in the L and C environments for component i, respectively. The dual L and C sorption contributions, in local equilibrium, are accounted for by this fundamental model. Model parameters ( $k_{C,i}$ ,  $C'_{L,i}$ ,  $b_i$ ,  $D_{Li}$ , and  $D_{Ci}$ ) can be estimated using simple pure gas measurements (5) and allow predictions for binary and more complex feeds with impurities. As will be shown later, using the estimated values for sorption affinity coefficients measured here at 700 and 900 C, the actual trends in pure vs. mixed gas CO<sub>2</sub> permeability at 800 C in Figure 2 can be explained.

This capability makes Equation 5a and b valuable tools, with trends in parameters giving insights into changes with pyrolysis temperature. During pyrolysis, in the hot inert environment, the Koros group has hypothesized that stressed random coil precursor polymer chain bonds can fragment during further aromatization (5-6). The resulting shorter rigid strands favor arrangement into plate-like structures, analogous to liquid crystal entropically driven phase transitions (7-8). In this environment distributed microporous volumes can provide the Langmuir (L) sorption term in Equation 4—shown as cubes in Figure 5, but other 3-d polygons are of course possible. The cubes are utilized to illustrate the Langmuir domain in a convenient manner, just for easy understanding. Such Langmuir domains are bounded by molecular sieving ultramicroporous walls, while the continuous “C” phase, comprising randomly oriented red strands in Figure 5, are the locus of Henry’s Law sorption.

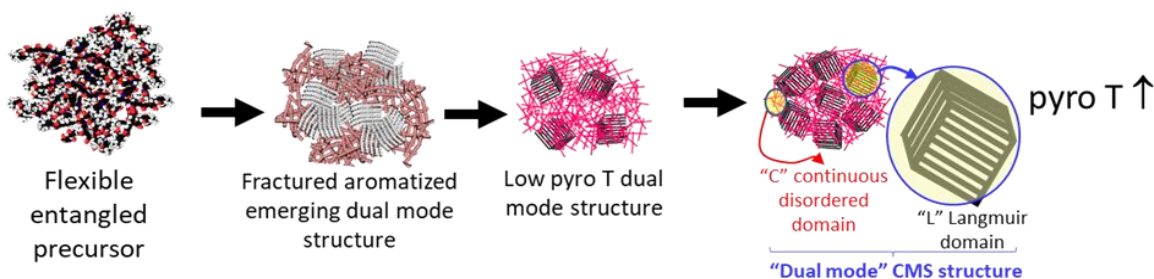


**Figure 5: Hypothetical vision showing self-consistent basis for developing CO<sub>2</sub>/CH<sub>4</sub> sorption selectivity and diffusion selectivity with increasing pyrolysis temperatures due to tighter Langmuir mode in a dual mode morphology with increasing pyrolysis temperatures.**

Fundamentally connecting properties of such a CMS morphology to the mechanism of its creation provides a *self-consistent framework* that extends from the molecular scale all the way to final membranes (5). The dual mode model parameter values and their trends with pyrolysis temperature will be shown to give insights into the pyrolysis process using the measurable, physically meaningful parameters ( $k_{C,i}$ ,  $C'_{L,i}$ ,  $b_i$ ,  $D_{Li}$ , and  $D_{Ci}$ ) for the L and C environments indicated in Figure 5. In fact, even before making actual measurements, *we envisioned partial exclusion of bulky CH<sub>4</sub> in Figure 5 from the Langmuir mode*, leading to an increasing trend in  $\alpha_S = S_{CO_2}/S_{CH_4}$  apparent from relative values of  $S_{CO_2}$  and  $S_{CH_4}$  in Figure 4ai-iii. This expectation meant that one should observe significant reductions in  $C'_{L,CH_4}$  with only small reductions in  $C'_{L,CO_2}$  with increasing pyrolysis temperature for L domains in the CMS (Figure 5). Indeed, such a trend may be reflected in the dual mode model related to Equations 5 a and b with trends in  $D_{Ci}$ ,  $D_{Li}$ , and  $F_i$  parameters indicative of increased diffusion selectivity for the CO<sub>2</sub>/CH<sub>4</sub> pair due to *increased entropic factors in diffusion* with increasing pyrolysis temperature. Results for other important gas pairs, studied only using indirect methods like those by Zhang also indicated trends like those in Figure 2 (9-12). This work predated the dual mode model for

CMS in Equation 5. In any case, such additional dual mode detail goes beyond an analysis based only on temperature dependence of *average diffusion coefficients like those in Figure 4a*. While this thesis focuses primarily upon the sorption selectivity topic (related to Equation 4), a related dissertation by a colleague, Nicholas Leon, will pursue such *dual mode diffusion issues* in detail. Even *without invoking diffusion features*, however, I will show later that Langmuir sorption affinity constants measured in my work correctly predict differences between pure and mixed gas CO<sub>2</sub> permeation behavior using Equation 5a. As will be shown, this is impressive proof of the fundamental importance of sorption effects in permeation behavior of CMS materials.

Another interesting illustration of the value of the self-consistent dual mode model can be noted by recalling the discussion of S<sub>CO<sub>2</sub></sub> and S<sub>CH<sub>4</sub></sub> at 100 psia in Figure 4ai-iii. Recall that these data were measured *indirectly by Zhang's work using Equations (1-3)* by calculating  $S_i = P_i/D_i$ ; however, such data can also be measured directly as  $C_A/p_A$  at 100 psia *as I do in the study*. It is significant that *limited direct measurement like mine were made many years ago by Kiyono, but only at 550°C*, which will be discussed briefly in Appendix A (13). I will show that directly measured S<sub>CO<sub>2</sub></sub> and S<sub>CH<sub>4</sub></sub> values at 100 psia show a pronounced maximum that was seen in Zhang's results suggested near 800 °C pyrolysis in Figure 4a-iii. Such a maximum suggests the existence of *two countervailing factors at play in the pyrolysis range between 550-900 °C*. My detailed dual mode sorption parameter results help explain this trend and may help understand the complex morphology changes in the important pyrolysis temperature range between 550 and 900 °C. I think my results emphasize the value of the self-consistent dual mode sorption model and its parameters in Equation 4. While indirect estimates of  $P_A$ ,  $P_B$ , and  $D_A$ ,  $D_B$ ,  $S_A$ , and  $S_B$  parameters are

valuable for screening as in Zhang's work, a prior study by Zimmerman et al (14) calls attention to limits related to such *indirect* estimates for a different polyimide precursor, 6FDA:BPDA-DAM.

Zimmerman et. Al (14) showed that trends in parameters can be discovered by indirect estimations, but the “gold standard” to understand phenomena is direct measurement such as used in this thesis. Zimmerman studied O<sub>2</sub>/N<sub>2</sub> CMS properties and showed that indirect estimates of  $D_{O_2}$  and  $\alpha_D = D_{O_2}/D_{N_2}$  differed by 37% and 56% respectively from directly measured results for  $D_{O_2}$  and  $\alpha_D = D_{O_2}/D_{N_2}$ , respectively that used  $P_{O_2}$ ,  $P_{N_2}$  and  $D_{O_2}$ , and  $D_{N_2}$ .

Nevertheless, the same *general trends* were followed for the directly measured parameters and the indirectly measured parameters, which supports the validity of the  $S_{CO_2}$  and  $\alpha_S = S_{CO_2}/S_{CH_4}$  trends in Figure 4a. Fortunately, I could use my actual directly measured  $S_{CO_2}$  and  $\alpha_S = S_{CO_2}/S_{CH_4}$  parameters in my analysis over the wide range of pyrolysis temperatures between 550-900 °C in my study. It was satisfying to see the same *general trends* in my directly measured 100 psia  $S_{CO_2} = C_{CO_2}/p_{CO_2}$  and  $\alpha_S = S_{CO_2}/S_{CH_4}$  and values apparent in Figure 4a.iii. Moreover, since the self-consistent model predictions are available using Equation (4) and Equation (5), for  $S_A = C_A/p_A$ ,  $S_B = C_B/p_B$ , and  $P_A$  and  $P_B$ , direct measurements of these parameters is preferred. This fact notwithstanding, indirect measurement of  $S_{CO_2} = C_{CO_2}/p_{CO_2}$  and  $\alpha_S = S_{CO_2}/S_{CH_4}$  are valuable to identify conditions on which to focus as Zhang did identify hypotheses to check. This is exemplified by my hypothesis in this thesis that the increase in  $\alpha_S = S_{CO_2}/S_{CH_4}$  at high pyrolysis temperature reflected sharp reductions in  $C'_{L,CH_4}$  with only small reductions in  $C'_{L,CO_2}$  as noted earlier.

In this regard, both indirect and direct estimation parameter approaches are complementary.

## 2.3 References

1. Zhang, C.; Koros, WJ, Ultraselective Carbon Molecular Sieve Membranes with Tailored Synergistic Sorption Selective Properties, *ADVANCED MATERIALS*, 29 (33), Article Number: 1701631(2017).
2. Koros, W. J., “Membranes and membrane processes”, *Encyclopedia of Chemical Processing and Design*, Ed. By J. J. McKetta, Marcel Dekker, New York, Vol. 29 (1988).
3. Saha, D., B A O, Z., Jia, F., Deng, S., Adsorption of CO<sub>2</sub>, CH<sub>4</sub>, N<sub>2</sub>O, and N<sub>2</sub> on MOF-5, MOF-177, and Zeolite 5A, *Environ. Sci. Technol.* 44, 1820–18 (2010).
4. Chapter 3, Section 3.1, Adsorbents-Fundamental and Applications, Sorbent selection, Yang, Wiley-Interscience, 2003.
5. Sanyal, O.; Hays, SS; Leon, NE, Guta, YA; Itta, AK; Lively, RP; William J. Koros, A Self-Consistent Model for Sorption and Transport in Polyimide-Derived Carbon Molecular Sieve Gas Separation Membranes, *Angew. Chem. Int. Ed.* 59, 20343 –20347 (2020).
6. Adams, JS; Itta, AK; Zhang C; Wenz, GB; Sanyal, O; Koros, WJ, New insights into structural evolution in carbon molecular sieve membranes during pyrolysis, *CARBON*, 141, 238-246 (2019).
7. P.J. Flory, Molecular theory of liquid crystals, *Adv. Polym. Sci.* 59 (1984).
8. Onsager, L, The effects of shape on the interaction of colloidal particles, *Annals of the NY Academy of Sciences*, 51(4) 627-659.

9. Singh, A. and W.J. Koros, “Significance of entropic selectivity for advanced gas separation membranes”, *I&EC Research*, 35, 1231-4 (1996).
10. Ning, X; Koros, W, Carbon molecular sieve membranes derived from Matrimid® polyimide for nitrogen/methane separation”, *Carbon*, 66, 511-522 (2014).
11. Rungta, M; Xu, L; Koros WJ, Carbon molecular sieve dense film membranes derived from Matrimid® for ethylene/ethane separation, *Carbon*, 50, 1488 –1502 (2012).
12. Fu, S.; Sanders, ES, Kulkarni, SS, Wenz, GB; Koros, WJ, Temperature dependence of gas transport and sorption in carbon molecular sieve membranes derived from four 6FDA based polyimides: Entropic selectivity evaluation, *CARBON*, 95, 995-1006 (2015).
13. Kiyono, M; Koros, WJ; Williams, PJ, Chapter 7, “Correlation between pyrolysis atmosphere and carbon molecular sieve membrane performance properties”, in Correlations in Membrane Science, Ed. By S. T. Oyama and S. S. Williams, Elsevier Science Publishers, *Advances in Membrane Science Series*, p. 137-171 (2011).
14. Zimmerman, CA; Sing A., Koros WJ, Diffusion in Gas Separation Membrane Materials: A Comparison and Analysis of Experimental Characterization Techniques, *Journal of Polymer Science: Part B: Polymer Physics*, Vol. 36, 1747–1755 (1998).

## CHAPTER 3. MATERIALS AND EXPERIMENTAL METHODS

A variety of different materials and procedures were relied upon by previously done work by members and alumni of the Koros group. The materials utilized and methods for all procedures and experimentation done in this study are the same as those previously done by those researchers/group alumni.

### 3.1 Formation of CMS Membranes

The polymer precursor utilized in the formation of the CMS thin film membranes tested in this research was Matrimid®. This precursor was purchased from Huntsman Chemicals and dried in a vacuum oven at 180°C for 24 hours before use. After this is completed, it is ready to be mixed with solvent to create solutions for film casting. The solvent utilized in this research was primarily Tetrahydrofuran (THF).

Details of membrane fabrication are provided in previous publications, but general procedures that were utilized will be discussed in this chapter. The precursor dense film membranes were prepared via a solution casting method. The precursor membranes were pyrolyzed in a quartz tube heated in a three-zone furnace. The pyrolysis protocols have also been discussed previously in various studies, but I will also discuss them in a later section and illustrate the process.

#### 3.1.1 Precursor Film Formation

After the polymer precursor was dried, solutions are prepared in 30 mL clear storage bottles and placed on a roll mill overnight to mix with THF. The polymer film was

then formed by pouring onto a mirrored plate under a vent hood, casted with a casting knife, and then allowed to spread and form a flat film shape overnight. After transporting from the vent hood, the film is then dried in a vacuum oven at 20°C. After this, the film is ready for pyrolysis to convert to CMS.

### 3.2 Pyrolysis Equipment and Protocol

A slotted quartz plate was used with each piece of precursor film placed on a quartz plate inside the pyrolysis furnace.

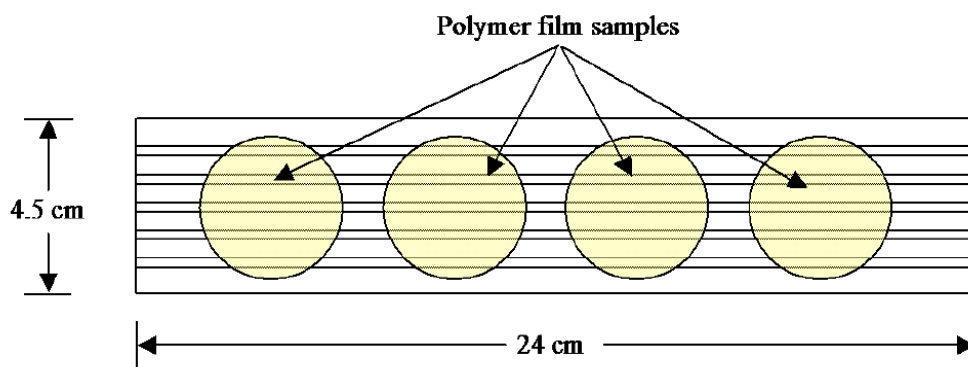


**Figure 6: Placement of flat, polymeric precursor films on a quartz plate for pyrolysis (1).**

To create the carbon molecular sieve membrane, a pyrolysis system was utilized. The setup consists of a furnace with three zones (Thermcraft), with each zone's temperature measured by a thermocouple, which is controlled by a multi-channel controller (Omega) to set the desired protocol and temperature profile. The furnace heats the film inside a quartz tube form National Scientific Company that are sealed with 2 silicon O-rings and 4 metal flanges. In addition to monitoring the temperature in the three different zones, the concentration of oxygen inside the tube is monitored by an oxygen analyser (Rapidox). This is critical to analyze as Argon is used to purge the system from oxygen

prior to pyrolysis, controlled with a mass flow controller. The main temperature of the films tested throughout the sorption tests were 550, 700, and 900 °C. The soak time, and pyrolysis protocol will be discussed in later sections.

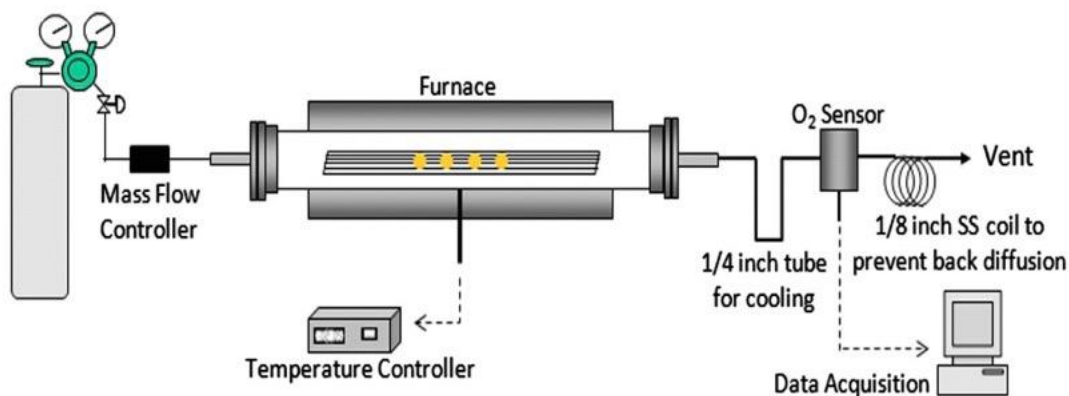


**Figure 7: Schematic of pyrolysis furnace and its setup**

### 3.2.1 Protocols

A variety of protocols are available to pyrolyze the polymer dense films to CMS dense films. The main protocols utilized for this work are seen below, along with the soak time, where the final temperatures ranged from 550 to 900 °C. Below are 3 tables exhibiting the pyrolysis protocols used over the course of this work.

**Table 1: CMS-550 Pyrolysis Protocol**

	<b>Temperature (°C)</b>	<b>Ramp Rate (°C/min)</b>	<b>Time (min)</b>
Setpoint	50		
Step 1	50	---	10
Step 2	250	13.3	15
Step 3	535	3.85	74
Step 4	550	0.25	60
Step 5	550	---	120

**Table 2: CMS-700 Pyrolysis Protocol**

	<b>Temperature (°C)</b>	<b>Ramp Rate (°C/min)</b>	<b>Time (min)</b>
Setpoint	50		
Step 1	50	---	10
Step 2	250	13.3	15
Step 3	685	3.85	113
Step 4	700	0.25	60
Step 5	700	---	120

**Table 3: CMS-900 Pyrolysis Protocol**

	<b>Temperature (°C)</b>	<b>Ramp Rate (°C/min)</b>	<b>Time (min)</b>
Setpoint	50		
Step 1	50	---	10
Step 2	250	13.3	15
Step 3	885	3.85	173
Step 4	900	0.25	60
Step 5	900	---	120

A key topic to avoid artifacts relates to furnace cleanliness which is managed using so-called “burnout.” The burnout protocol was utilized between each CMS preparation protocol to ensure the tube is clean of all emissions released from the Matrimid® throughout its conversion to CMS. The burnout period removes impurities inside of the tube, basically resetting the system, and preparing it for another round of pyrolysis to prepare film for either permeation or sorption. The burnout protocol can be referenced on the following page.

**Table 4: Burnout Protocol**

	<b>Temperature (°C)</b>	<b>Ramp Rate</b>	<b>Time (min)</b>
Setpoint	50		
Step 1	50	---	10
Step 2	900	8.5	100
Step 3	900	---	200

*3.2.2 Additional comments on pyrolysis protocols*

Besides the above-mentioned burnout protocol, before a pyrolysis, the metal fittings comprising the pyrolysis furnace were broken down into their individual Swagelok parts and flanges. These pieces were then placed in n-methyl pyrrolidone, (NMP), and heated to approximately 100 °C for at least 6 hours. The pieces were then cooled and dried before being placed in water and then acetone for 6 hours each. Then they were dried at approximately 200 °C overnight. NMP and acetone were both purchased from Sigma-Aldrich, (St. Louis, MO). After cleaning, another standard burnout procedure was used (2). Before the actual burnout protocol, both the quartz tube and stainless-steel mesh were rinsed with acetone to remove any visible remnants from previous pyrolysis runs. The furnace parts, both the ones cleaned with NMP and the quartz tube, were then connected with the slotted quartz support plate sealed inside the furnace. While tedious such protocols were felt to be wise to avoid any artifacts noted in prior work (3).

### 3.3 Sorption Methodology

Gas sorption measurements were made using a pressure decay method (4, 5). CMS dense films were used for the sorption tests, and the flat sheet membranes were gently broken into small pieces (as mentioned in an earlier section) between two pieces of weighing paper. The CMS pieces were loaded into a stainless-steel Swagelok filter element and wrapped loosely by aluminum foil to ensure that the samples remained in the filter. The sorption apparatus was placed in a temperature-controlled oil bath (see Figure 8). The system was evacuated for 24 hours prior to testing, then feed gas was introduced into the reservoir chamber and allowed to equilibrate for 10–15 min. The thermally equilibrated gas was then introduced into the sample cell and the pressures in the sample cell and reservoir were monitored by pressure transducers and recorded over time using LabVIEW. Sorption isotherms were then obtained for the equilibrium sorbed gas concentration at each final pressure. Each film was tested at roughly 4-7 different pressure levels, increasing from 50 psi to 500 psi. Pure gas sorption isotherms are determined using our pressure-decay sorption equipment, shown as a photo and a schematic for clarity in the discussion. The oil bath allows the sorption test temperature ranging from room temperature up to 100 °C; however, in this work, only 35 °C was studied.

A schematic of one of the current 26 sorption systems used in the Koros group is shown below in Figure 8. Since this has been described in earlier publications, only a summary discussion of the unit is described here.

As described above, CMS dense films were gently broken into small pieces (as mentioned in an earlier section) between two pieces of weighing paper. The CMS pieces

were loaded into a stainless-steel Swagelok filter element and wrapped loosely by aluminum foil to ensure that the samples remained in the filter. The sorption apparatus was placed in a temperature-controlled oil bath, for this study, 35 °C. The system was evacuated for 24 hours prior to testing, then feed gas was introduced into the reservoir chamber and allowed to equilibrate for 10–15 min. The thermally equilibrated gas was then introduced into the sample cell and the pressures in the sample cell and reservoir were monitored by pressure transducers and recorded over time using LabVIEW. Sorption isotherms were then obtained for the equilibrium sorbed gas concentration at each final pressure. Each film was tested at roughly 4-7 different pressure levels, increasing from 50 psi up to 500 psi.

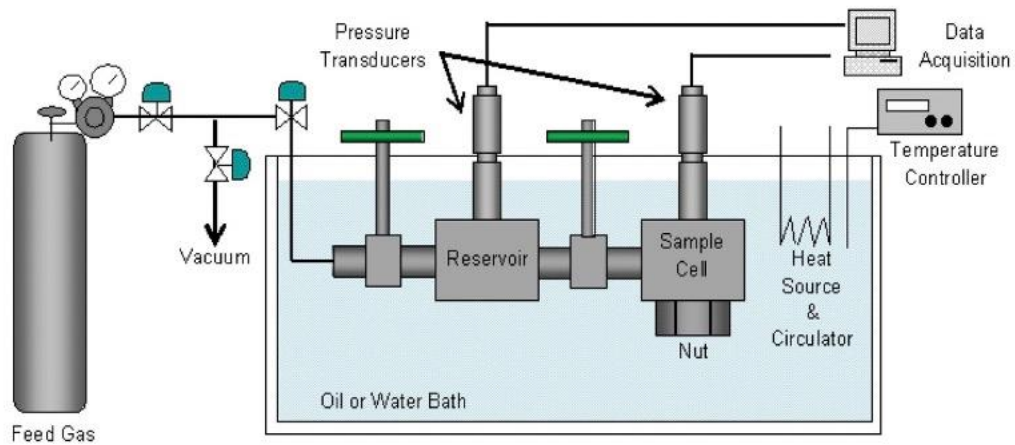


**Figure 8: Schematic of pressure decay sorption system that was used throughout the entirety of this work.**

The pressure transducers allow precise measurement of pressures in reservoir and sample cell volume. The transducers convert pressure to a digital signal which is displayed

on a digital multimeter or recorded in LabView. The pressures of the cell and reservoir are recorded. Then, gas is introduced into the sample chamber (i.e., cell) by opening the connecting valve for approximately 1 second. Once this valve is closed, the pressure in the sample chamber will decay due to gas sorption into the sample. After the pressure equilibrates, the pressures are recorded again. Equilibrium is signaled when the pressure in the cell remains constant with no decreasing trend for 1-3 hours. The amount of gas,  $j$ , that resides in the CMS sample with volume  $V_s$  is given by the following Equation (4), and  $C_j = (n_{jS}/V_p) \times 22400 (=) \text{cc(STP)/cc CMS}$ .

$$n_s = \frac{1}{R_g T} \left[ (V_C - V_S) \left( \frac{p_{C,i}}{z(p_{C,f})} - \frac{p_{C,f}}{z(p_{C,f})} \right) + V_R \left( \frac{p_{R,i}}{z(p_{R,i})} - \frac{p_{R,f}}{z(p_{R,f})} \right) \right] \quad (6)$$

where  $n_{iS}$  is the number of moles of “ $j$ ” sorbed in the CMS sample,  $R_g$  is the ideal gas constant,  $T$  is temperature, and  $V_R$ ,  $V_C$ , and  $V_S$  are the volumes of the reservoir, sample cell and sample, respectively. The externally applied pressure is denoted by  $p$  and  $z$  is the corresponding compressibility. The subscripts “ $C$ ” and “ $R$ ” refer to the cell and reservoir in Figure 8, respectively and the subscripts “ $i$ ” and “ $f$ ” refer to initial (before opening valve to the sample volume) and final (after opening this valve) states. The system is interfaced with a personal computer running National Instruments LabView™ software, which allows for visualization of the pressure decay and equilibrium and for data collection. The volumes of the reservoir and cell and total sorption concentration can be determined to within + 0.5%. The pressure in the reservoir is then changed and the cycle is repeated until the isotherm is completed.

To attempt to expedite the experiments, several sorption systems were used for measurements, but only the results from one of the systems is reported here. Specifically, after collecting the pressure decay data, it was discovered that volumes of two of the cells were incorrect, due to a record-keeping error during the period of COVID-19 operations. This disturbing fact was discovered only after all the pressure data were collected over a period of 4 months before the actual calculations were done. This approach will not be followed in the future and calculations will be done as soon as possible. Fortunately, one of the three cells had been calibrated by a postdoc in the group and the results were verified using a separate independent sample measurement. Only the results from that verified cell (System I) were used here in the main body of my thesis. The pressure data for the other system II and III are recorded in Appendix B, and I plan to use these additional data, along with the current data reported from System I when the final paper on my work is submitted for journal publication.

Another hurdle was also encountered that prevented my original plans to run a limited number of sorption isotherms to estimate the enthalpies of sorption from the temperature dependences of the affinity coefficients and Henry's Law coefficients. This planned work is omitted from this thesis, but Nicholas Leon will continue and complete this in his PhD work.

### 3.4 References

1. Vu, De, Chapter 3, Formation and Characterization of Carbon Molecular Sieve and Mixed Matrix Membranes for Natural Gas Purification, University of Texas at Austin, PhD Dissertation, 2001.
2. Kiyono, M; Koros, WJ; Williams, PJ, Chapter 7, “Correlation between pyrolysis atmosphere and carbon molecular sieve membrane performance properties”, in *Correlations in Membrane Science*, Ed. By S. T. Oyama and S. S. Williams, Elsevier Science Publishers, Advances in Membrane Science Series, p. 137-171 (2011).
3. Sanyal, O; Hicks, ST; Bhuvania, N; Hays, S; Kamath, MG; Karwa, S., Swaidan, R; Koros, WJ, Cause and effects of hyperskin features on carbon molecular sieve (CMS) Membranes, *Journal of Membrane Science* 551 (2018) 113–122.
4. Koros, WJ; Paul, DR, Design considerations for measurement of gas sorption in polymers by pressure decay, *J. Polym. Sci.: Part B: Polym. Phys.*, 14, 1903-1907 (1976).
5. Costello, L. M.; Koros, W. J., Temperature-dependence of gas sorption and transport-properties in polymers – measurement and applications. *Industrial & Engineering Chemistry Research* 1992, 31 (12), 2708-2714.

## CHAPTER 4. CHARACTERIZATION OF MATRIMID® CMS

### 4.1 Overview

The focus of this thesis is on 35 °C gas sorption and its interpretation using the dual mode sorption model as tool for morphology analysis in CMS membranes. Nevertheless, more traditional complementary characterizations using materials science tools are considered briefly. This approach is discussed first to show that although traditional tools add information, they lack the ability to give significant insight without the dual mode model framework. Besides summarizing Zhang's work (1), additional characterization using XPS was done to provide insights into elemental analysis of CMS dense films. This work was kindly done by Dr. Zhongyun Liu using a Thermo K-Alpha XPS with an X-ray beam size of 400 nm for the 550, 700 and 900 °C pyrolyzed CMS samples. Like the more traditional materials science characterizations results of Zhang to be discussed, these XPS results also add marginal additional unambiguous insights *until the dual mode sorption framework is considered*. Before presenting the new XPS results, the background insights from Zhang (1) will be discussed from his article.

### 4.2 Traditional Pore Size Characterization Using CO<sub>2</sub> Physisorption

Pore-size distribution characterization (1) using 273 K CO<sub>2</sub> sorption used by Zhang in his CMS membranes (2) in Figure 9a-e indicate pore sizes up to 10.83 Å), pore sizes of the CMS membranes, with reduced pore sizes as pyrolysis temperature increases. The peak at around 5.5 Å for the sample pyrolyzed 750 and 800 °C is clear. Also, evidence of 4.5–5.0 Å is present and becomes stronger for pyrolysis from 850 to 900 °C. Moreover, evidence

for a still smaller peak related to 4.0–4.5 Å features in the CMS pyrolyzed at 875 and 900 °C appears. This peak, shifted to lower pore-size range as pyrolysis temperature grows from 875 to 900 °C suggests the presence of smaller pores as pyrolysis temperature increases. This trend may be consistent with my suggested interpretation of Figure 5 but is not definitive; whereas the dual mode model Equation (4) and Equation (5) provides insight that may be ultimately connected to diffusion coefficients, which is beyond the scope of this work.

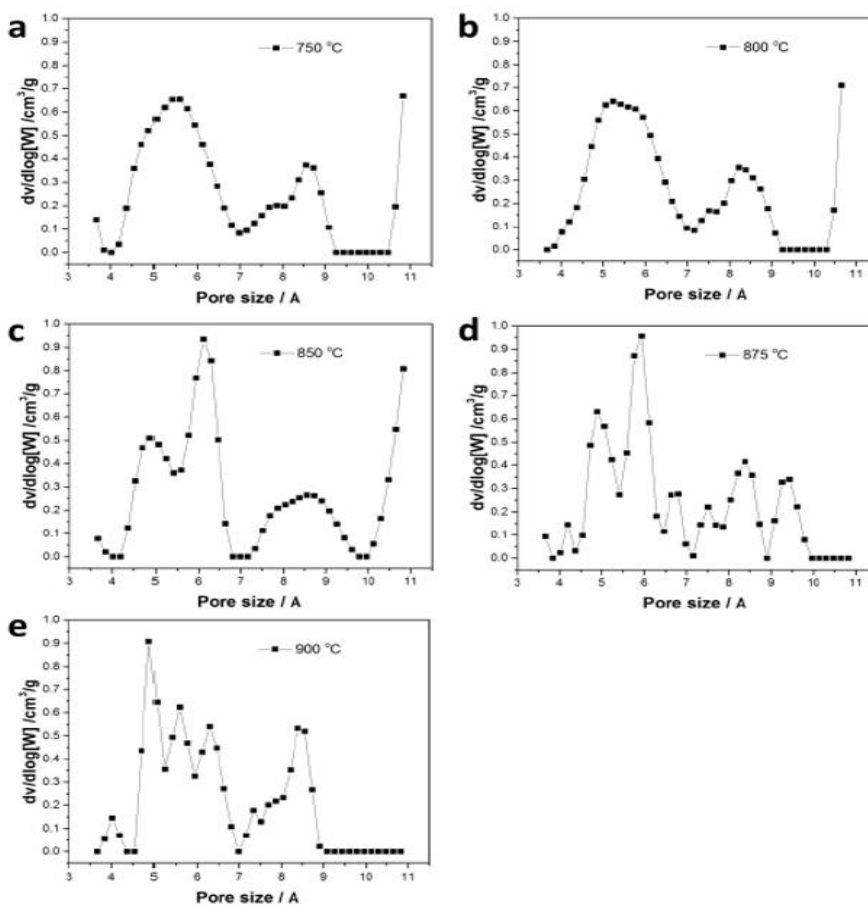


**Figure 9a, b, c, d, e:  $dV/d\log W$  (differential pore volume) vs. pore size ( $W$ ) for CMS Membranes pyrolyzed at (a) 750 °C, (b) 800 °C, (c) 850 °C, (d) 875 °C, (e) 900 °C.**

### 4.3 Morphology Characterization Using WAXD and RAMAN Spectroscopy

The Figures 9a-e pore size characterizations and Zhang's wide-angle X-ray diffraction (WAXD) results in Figures 4a-b (2) are consistent with a highly amorphous structure of CMS comprising a highly disordered amorphous material. Also, Zhang's Raman spectroscopy (2) results in Figures 10a-b, show D ( $1310\text{ cm}^{-1}$ ) and G ( $1595\text{ cm}^{-1}$ ) band peaks in the CMS membranes that are associated with the presence of non-graphitic D peaks and ordered graphitic-like  $\text{sp}^2$  carbon structure in the formed CMS membranes. Figure 4a and Figure 4b offer facts, but do not offer definitive insights regarding morphology. Figures 4a-b and the  $35\text{ }^\circ\text{C}$  sorption results that comprise the focus of my thesis using the dual mode framework do offer such insights as will be shown.

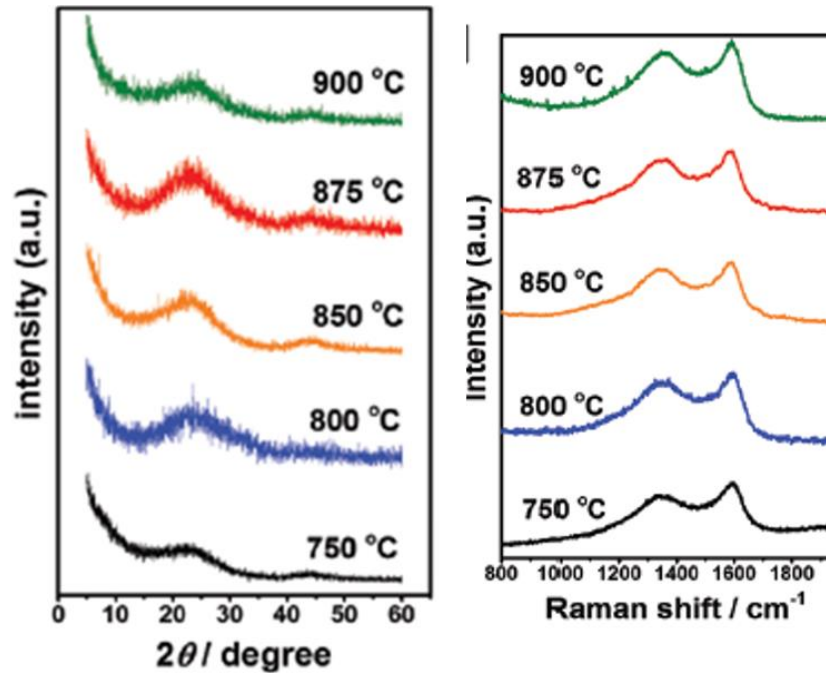


**Figure 10a, b: (a)Wide-angle X-ray diffraction (WAXD) and (b) Raman spectroscopy results for Matrimid®-derived CMS pyrolyzed under inert Argon from 750 –900 °C.**

#### 4.4 Matrimid® CMS Dense Film Scanning Electron Microscopy Imaging

To avoid any possible complications associated with artifacts due to asymmetric membrane structures, in this fundamental study, dense precursor Matrimid® film samples were used. To verify that the CMS cross section of my samples were featureless, except at the molecular scale, Figure 11, was kindly provided by Dr. Zachary Campbell in the Koros group. Higher resolution TEM features with dimensions approaching those Figure 5 have been reported (3); however, the features are lacking the resolution or ability to be interpreted to give real insight into morphology like that postulated and discussed here. Our perspective is that the CO<sub>2</sub> physisorption results in Figure 9 and detailed sorption analyses in terms of dual mode parameters discussed in Chapter 5 provide consistent and a more physically visualizable morphology to connect to membrane properties.

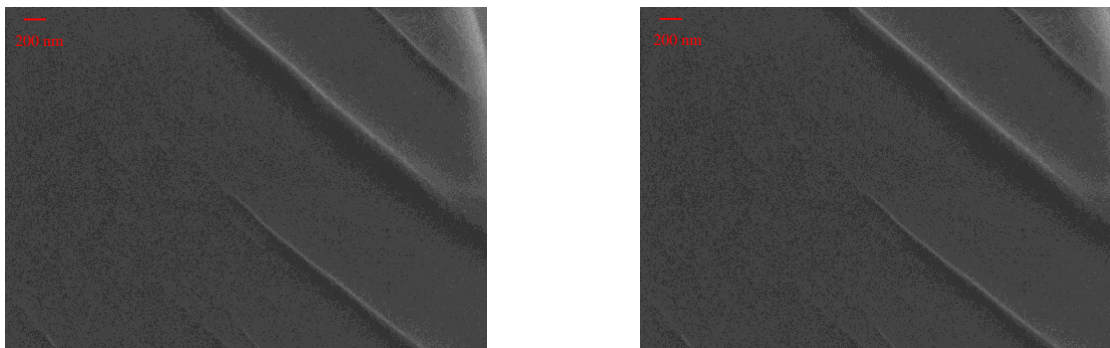


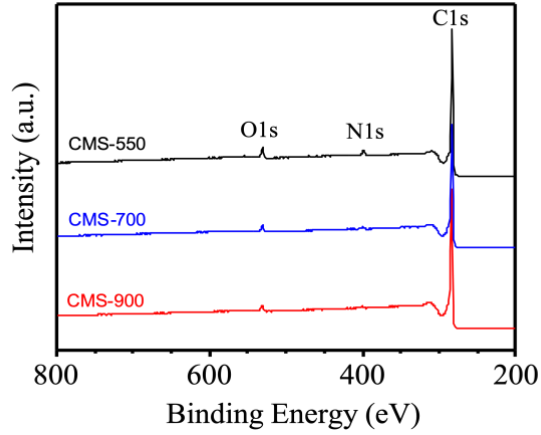
**Figure 11: SEM images of Matrimid® CMS-550 edge and surface, respectively. Verifies lack of apparent features at the microscale.**

#### 4.5 Characterization of Matrimid® CMS Dense Films using XPS

In an attempt to seek more insight, elemental characterization beyond that reported by Zhang (2) for Matrimid®-derived CMS, was pursued. This work was inspired by work of Liu (3) who studied a more complicated precursor than Matrimid®. I collaborated with Dr. Liu to perform XPS studies to further assess the chemical nature and composition to seek insights regarding the carbon nature of the CMS and its evolution for pyrolysis from 550 to 900 °C. These results are reported and discussed next. Like the WAXD and RAMAN spectroscopy results, it seems that although XPS offers facts, it still offers less physical insight regarding morphology than Figure 4a-e and the 35 °C sorption results that comprise the focus of my thesis.

For the elemental analysis in CMS dense films, a Thermo K-Alpha XPS with an X-ray beam size of 400 mm was used. Figure 12 show the atomic composition of Nitrogen in Matrimid® CMS-550 membrane significantly decreases upon pyrolysis above 550 °C, indicating that possibly the strands in the CMS tighten up, causing the CO<sub>2</sub>/CH<sub>4</sub> selectivity to improve. This would be consistent with the results that are presented in following chapters. Most of the Nitrogen is removed from the sampling by the time 900 °C is reached, presumably indicating the removal of any pyrrolic and pyridinic N groups at the highest pyrolysis temperatures. Another aspect to note is that sp<sup>2</sup> Carbon levels increase with increased pyrolysis temperatures. It is suggested that further XPS testing be done on multiple samples to achieve repeatability and to form a better picture as far as trends. Preliminary studies of pyridinic and pyrrolic groups are underway and will be include in the actual paper derived from this thesis. See the figures below. To further illustrate the

significant Nitrogen removal during pyrolysis, in a study conducted by Guiver, et al., it was found that Matrimid® polymer is composed with roughly 4.45% Nitrogen (4).



Membrane	C (Atomic%)	O (Atomic%)	N (Atomic%)
CMS-550	91.78	4.56	3.66
CMS-700	95.71	3.03	1.26
CMS-900	96.56	2.93	0.51

**Figure 12: Atomic Composition Results from XPS in Matrimid® CMS-550, 700, and 900 °C**

## 4.6 References

1. Wei, YJ; Wang, JC; Gu, C; Ma, Z, The Relationship between CO<sub>2</sub> Adsorption and Microporous Volume in a Porous Carbon Material, 56(6), 932-940 (2021).
2. Zhang, C; Koros, WJ, Ultraselective Carbon Molecular Sieve Membranes with Tailored Synergistic Sorption Selective Properties, *Advanced Materials*, 29 (33), Article Number: 1701631(2017).
3. Liu, ZY; Qiu, WL; Quan, WY; Koros, WJ, Advanced carbon molecular sieve membranes derived from molecularly engineered cross-linkable copolyimide for gas separations-) *Nature Materials*, 22 (1), 109-116 (2023).
4. Guiver, M.D., Robertson, G.P., Dai, Y., Bilodeau, F., Kang, Y.S., Lee, K.J., Jho, J.Y. and Won, J. (2002), Structural characterization and gas-transport properties of brominated matrimid polyimide. *J. Polym. Sci. A Polym. Chem.*, 40: 4193-4204. <https://doi.org/10.1002/pola.10516>.

## CHAPTER 5. CO<sub>2</sub>/CH<sub>4</sub> SORPTION IN MATRIMID®-DERIVED CMS

### 5.1 Introduction

Sorption isotherms are reported here at 35 °C for both CO<sub>2</sub> and CH<sub>4</sub> measured for CMS created under inert pyrolysis atmospheres at 550°C, 700°C, and 900 °C as described in Chapter 4 for Matrimid® precursors (See Scheme 1, in Chapter 1). Besides calculation of  $S_{CO_2} = C_{CO_2} / p_{CO_2}$  and  $S_{CH_4} = C_{CH_4} / p_{CH_4}$  at the 100 psia pure gas conditions between 750 and 900 °C pyrolysis temperatures in Figure 4a-iii, these data allow determination of the complete array of dual mode sorption parameters in Equation (4). Recall,  $k_{C,i}$  is the continuous mode Henry's law sorption constant of component  $i$ ;  $C'_{L,i}$  is the Langmuir sorption capacity;  $b_i$  is the Langmuir affinity constant, and  $f_i$  is the local fugacity of while  $K_i = \frac{C'_{L,i} b_i}{k_{C,i}}$  for both  $i = CO_2$  and  $CH_4$  at 35 °C in Equation 4 in Chapter 2:

$$C_i = C_{C,i} + C_{L,i} = k_{C,i} f_i + \frac{C'_{L,i} b_i f_i}{1 + b_i f_i} \quad (4)$$

These results are shown in Figures 13a and b, Figures 14a and b, through 15a and b and summarized in Figures 16a and b with a detailed listing of the associated dual mode parameters tabulated in Tables 5-7.

## 5.2 CO<sub>2</sub> Sorption Results

Below are figures that illustrate the dual-mode sorption isotherms for all three-pyrolysis temperature prepared Matrimid® dense films at various CO<sub>2</sub> pressure feeds. Discussion will follow the CH<sub>4</sub> sorption isotherms are shown.

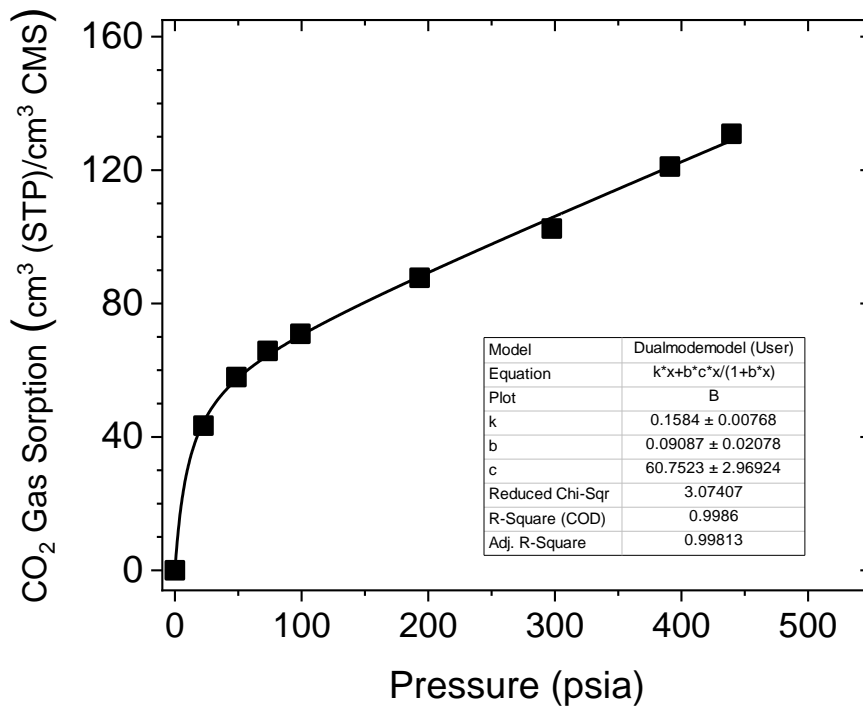


**Figure 13a: CMS-550 CO<sub>2</sub> Sorption Results at 35 °C**

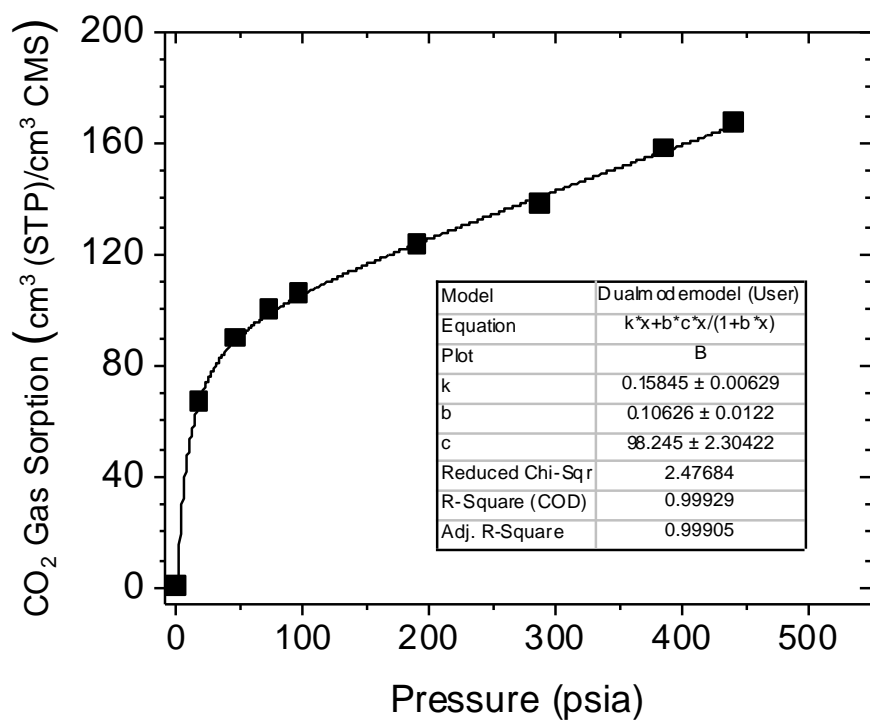


**Figure 13b: CMS-700 CO<sub>2</sub> Sorption Results at 35 °C**

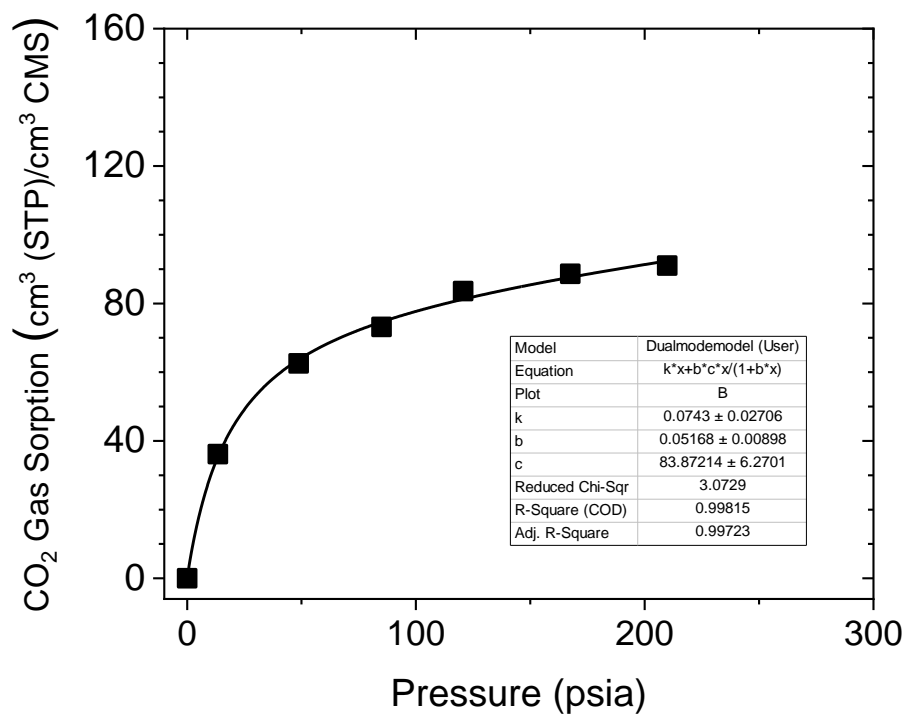


**Figure 13c: CMS-900 CO<sub>2</sub> Sorption Results at 35 °C**

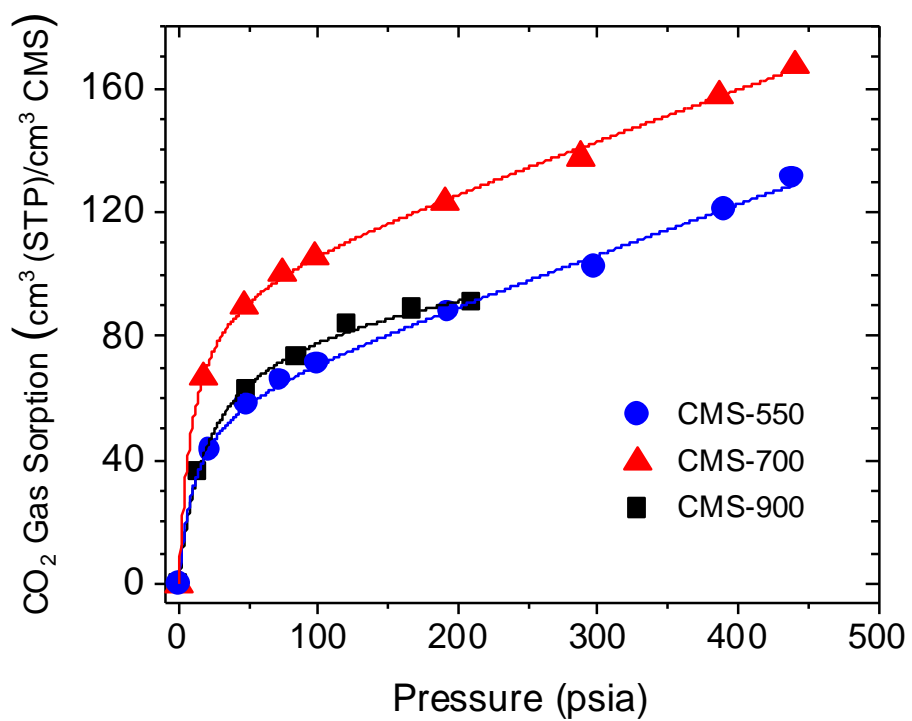


Figure 13d: Summary CO<sub>2</sub> Sorption Results for CMS-550, 700, and 900 at 35 °C

### 5.3 CH<sub>4</sub> Sorption Results

Below are figures that illustrate the dual-mode sorption isotherms for all three-pyrolysis temperature prepared Matrimid® dense films at various CH<sub>4</sub> pressure feeds. Discussion of these results will follow in the upcoming sections.

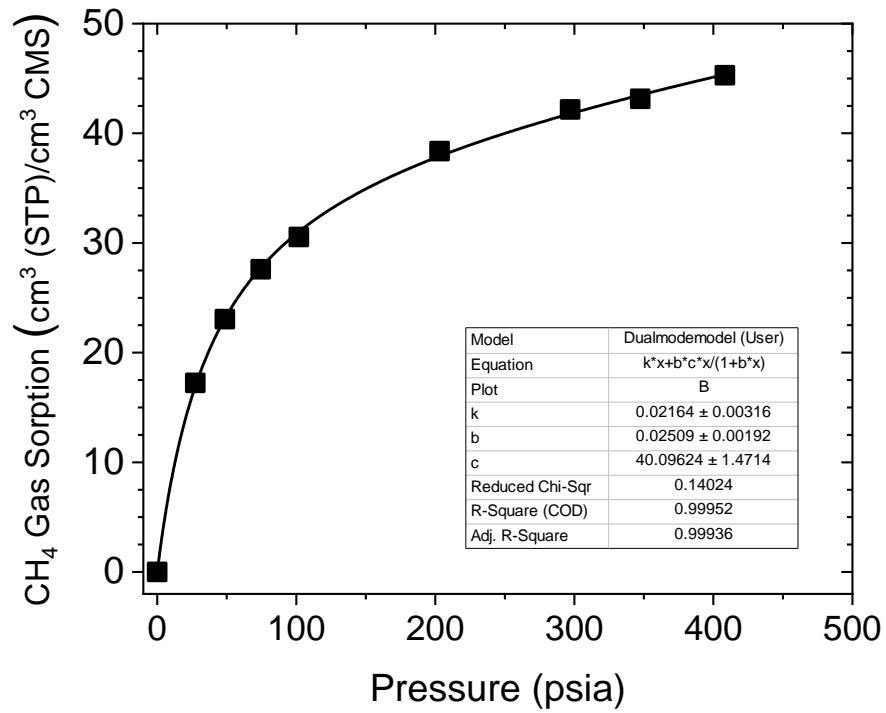
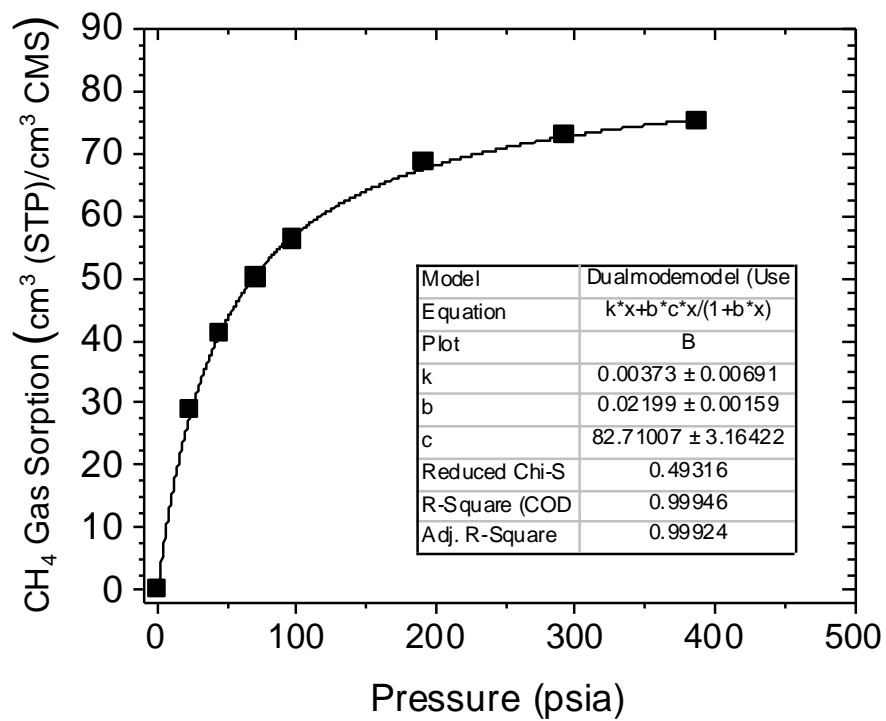


Figure 14a: CMS-550 CH<sub>4</sub> Sorption Results at 35 °C



**Figure 14b: CMS-700 CH<sub>4</sub> Sorption Results at 35 °C**

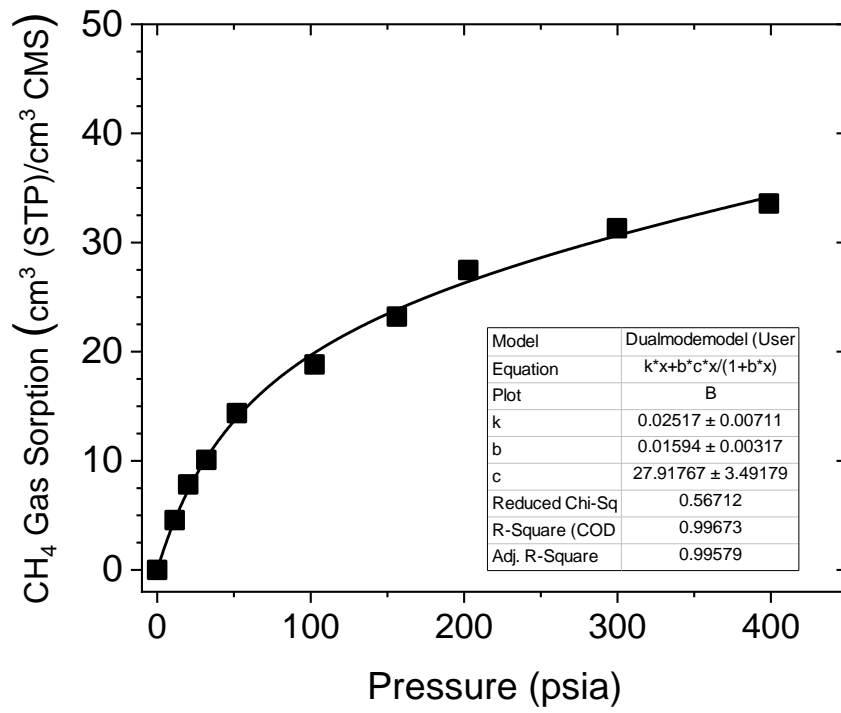
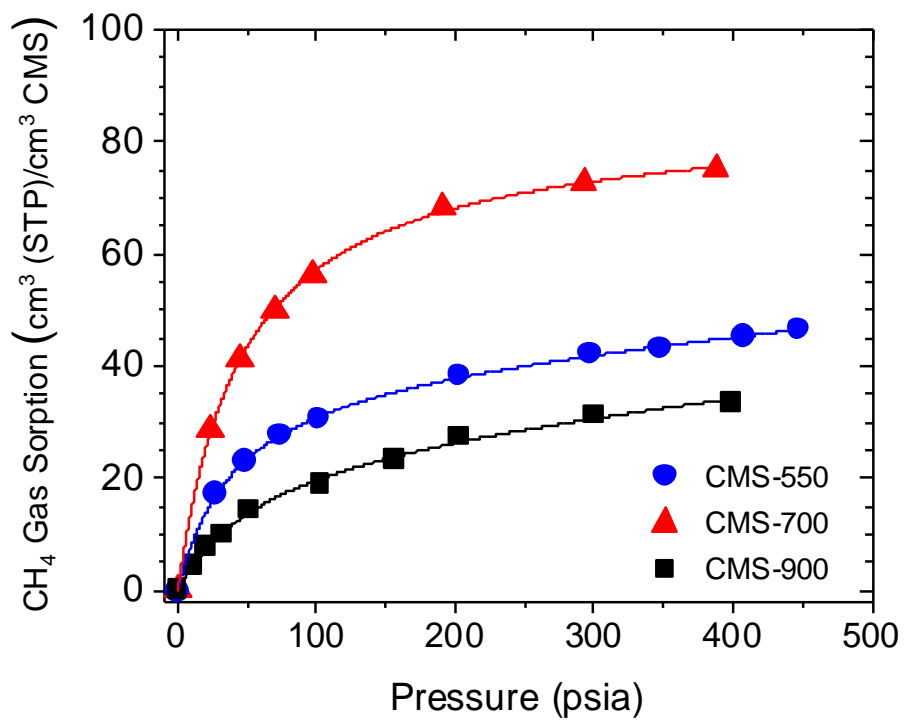


Figure 14c: CMS-900 CH<sub>4</sub> Sorption Results at 35 °C



**Figure 14d: Summary CH<sub>4</sub> Sorption Results for CMS-550, 700, and 900 at 35 °C**

## 5.4 Dual Mode Parameters

As mentioned in Chapter 2, the dominant feature behind observing the general trend is  $C'_{L,i}$  reaching a maximum for both CO<sub>2</sub> and CH<sub>4</sub>. The decrease is drastic for methane, which explains the selectivity and sorption coefficients that were directly measured throughout this experimentation.

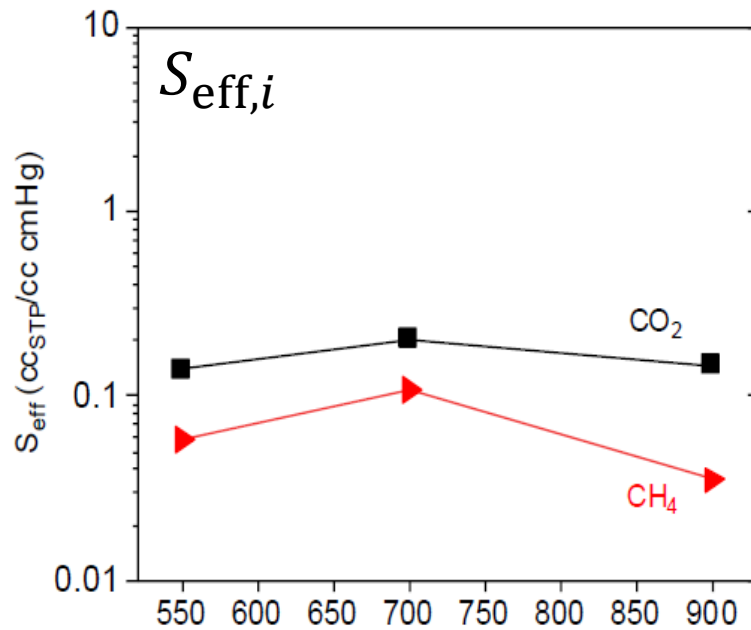


**Figure 15a:**  $S_{CO_2} = C_{CO_2}/p_{CO_2}$  and  $S_{CH_4} = C_{CH_4}/p_{CH_4}$  at 100 psia vs.  $T_{pyrolysis}$  at 550, 700 and 900 °C

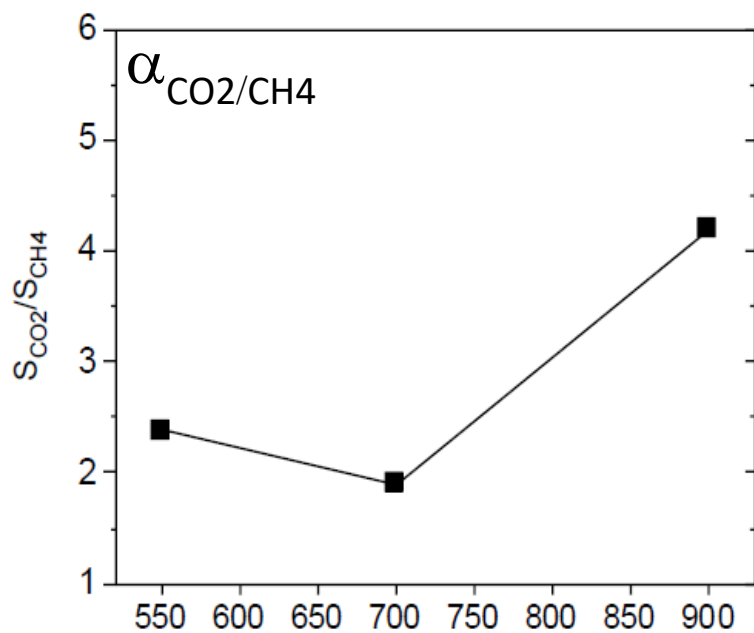


**Figure 15b:  $\alpha_S = S_{CO_2}/S_{CH_4}$  vs.  $T_{pyrolysis}$  at 550, 700 and 900 °C**

Dual mode sorption parameters from each pyrolysis temperature and each respective penetrant are also reported below.

**Table 5: Dual-mode sorption parameters for CO<sub>2</sub> and CH<sub>4</sub> Matrimid® CMS-550 dense film membranes. Isotherms were measured at 35 °C.**

Penetrant	$c'_{Li}$	$b$	$k_{C,i}$	K
CO <sub>2</sub>	60.75 ± 2.97	0.091 ± 0.021	0.158 ± 0.008	34.7 ± 2.56
CH <sub>4</sub>	40.10 ± 1.47	0.025 ± 0.002	0.022 ± 0.003	46.2 ± 3.12

**Table 6: Dual-mode sorption parameters for CO<sub>2</sub> and CH<sub>4</sub> Matrimid® CMS-700 dense film membranes. Isotherms were measured at 35 °C.**

Penetrant	$c'_{Li}$	$b$	$k_{C,i}$	K
CO <sub>2</sub>	98.25 ± 2.30	0.106 ± 0.012	0.158 ± 0.006	65.9 ± 4.21
CH <sub>4</sub>	82.71 ± 3.16	0.022 ± 0.002	0.004 ± 0.007	488.0 ± 8.76

**Table 7: Dual-mode sorption parameters for CO<sub>2</sub> and CH<sub>4</sub> Matrimid® CMS-900 dense film membranes. Isotherms were measured at 35 °C.**

Penetrant	$c'_{Li}$	$b$	$k_{C,i}$	K
CO <sub>2</sub>	83.87 ± 6.27	0.0517 ± 0.009	0.074 ± 0.027	58.3 ± 2.89
CH <sub>4</sub>	27.92 ± 3.49	0.0159 ± 0.0032	0.025 ± 0.007	17.68 ± 1.98

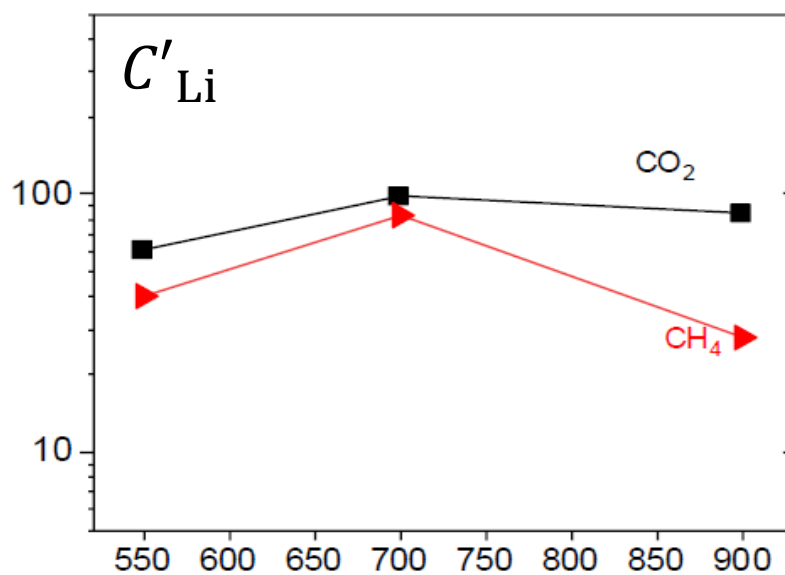


**Figure 16a:  $C'_{L,i}$  versus  $T_{pyrolysis}$  at 550, 700 and 900 °C**

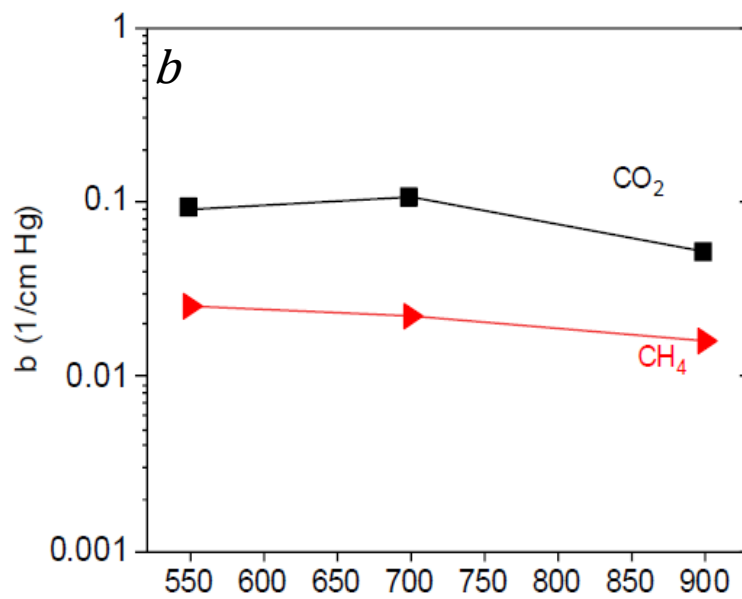


**Figure 16b:  $b$  (affinity constant) versus  $T_{\text{pyrolysis}}$  at 550, 700 and 900  $^{\circ}\text{C}$**

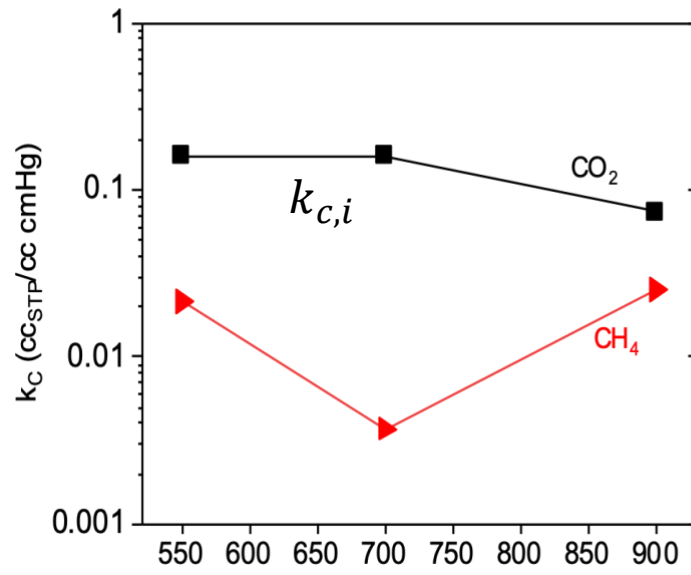


Figure 16c:  $k_{c,i}$  versus  $T_{\text{pyrolysis}}$  at 550, 700 and 900  $^{\circ}\text{C}$

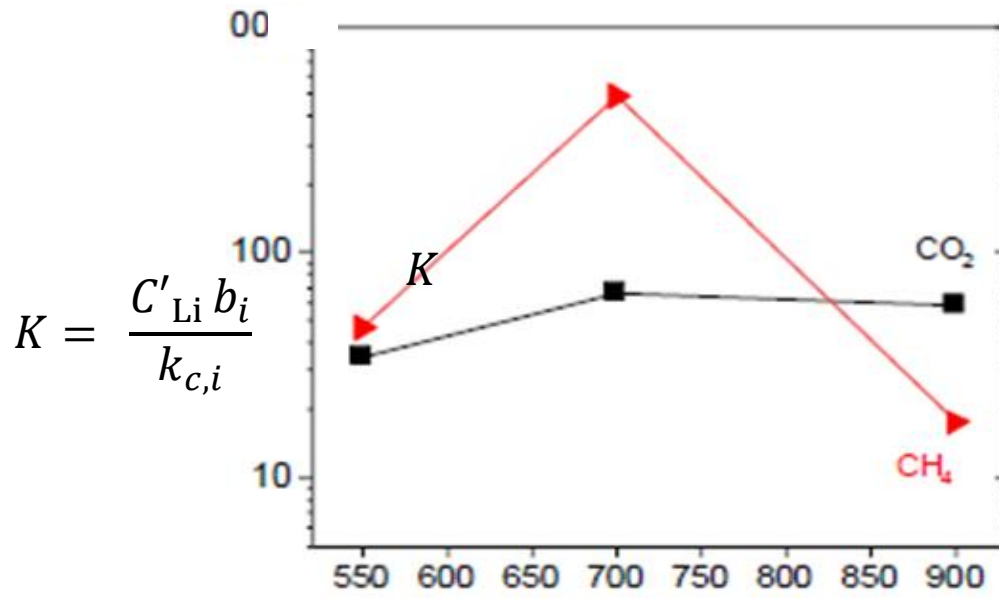


Figure 16d: K versus T<sub>pyrolysis</sub> at 550, 700 and 900 °C

## 5.5 Discussion

The general consistency of the trend in Figure 15a for  $S_{CO_2}$  and  $S_{CH_4}$  at 100 psia and 35 °C for pyrolysis temperatures from 750-900 °C is satisfying. Consistency with a sharp increase in sorption selectivity vs. pyrolysis temperature at 900 °C should also be noted in Figure 15b. My data in Figure 15a and 15b go beyond the range in Figure 2 from 550-900 °C and emphasize the trend seen versus pyrolysis temperatures. Furthermore, hypothesized exclusion selectivity, as the ultramicropores in the dispersed Langmuir mode walls tighten at higher temperature, are indicated. It is satisfying to see the dual mode sorption parameters at elevated temperature to reflect my hypothesis related to Equation (4) and the hypothesized cause for the trends observed in Figure 4. Specifically, the general reduction in the  $C'_{L,i}$ , Langmuir capacity, with increasing pyrolysis temperature is stronger for  $CH_4$  than for  $CO_2$ . This is also consistent with exclusion selectivity noted in Figure 4a and suggested in general in Figure 4b. The dual mode model now allows more detail in this picture, *and predicts increased molecular sieving related to the diffusion coefficient factors in Equation (5)*. This later diffusion topic, as noted earlier, will be explored by a study mentioned earlier by another Koros group member.

While changes in the  $k_{C,i}$  and  $b_i$  parameters with pyrolysis temperature are tempting to assign to evolution suggested in Figure 5, I will defer speculation until more detailed information regarding XPS results and  $CO_2$  physisorption results covering the full range of pyrolysis temperatures from 550-900 °C are available. We anticipate having such data provided by my colleague Dr. Zhongyun Liu before actual publication based on my thesis in a referred journal article.

Two final additional useful items merit discussion related to the above results in Section 5.1. The first item involves the use of the tabulated affinity constants for CO<sub>2</sub> and CH<sub>4</sub> to explain the trend in the 90:10 CO<sub>2</sub>:CH<sub>4</sub> mixed gas feeds for 100 psia total pressure with vacuum downstream. Figure 2 shows that mixed CO<sub>2</sub> permeabilities exceed pure gas CO<sub>2</sub> permeabilities, rather than showing CO<sub>2</sub> permeation suppression, which might be expected due to simple competition for the Langmuir capacity. Although it is beyond the sorption focus of the current thesis, the results merit discussion to show the power of the dual mode model framework in Equations 4 and 5. The concept of “local equilibrium,” connecting independently measurable equilibrium thermodynamic properties to local chemical potential gradients driving permeation at any given distance  $x$  through the membrane, are the basis for these equations. For the mixed gas (10%) CO<sub>2</sub>/CH<sub>4</sub> (90%) mixed-gas permeation at 35 °C and 100 psia feed pressure (vacuum downstream) the ratios pure and mixed gas CO<sub>2</sub> permeabilities in such a case gives the result:

$$[P_{CO_2}]_{10:90} / [P_{CO_2}]_{pure} = \frac{[1 + \frac{F_{CO_2}K_{CO_2}}{1 + b_{CO_2}p_{CO_2} + b_{CH_4}p_{CH_4}}]}{[1 + \frac{F_{CO_2}K_{CO_2}}{1 + b_{CO_2}p_{CO_2}}]} = \frac{[1 + \frac{F_{CO_2}K_{CO_2}}{1 + b_{CO_2}p_{CO_2} + b_{CH_4}p_{CH_4}}]}{[1 + \frac{F_{CO_2}K_{CO_2}}{1 + b_{CO_2}p_{CO_2}}]}$$

for any value of  $F_{CO_2} > 0$  and  $K_{CO_2} > 0$ , and  $b_{CO_2} > b_{CH_4}$  with  $p_{CO_2} = 10$  psia and  $p_{CH_4} = 90$  psia, the above ratio will be  $> 1$ , consistent with Figure 2. The specific ratio, of course, depends upon the value of  $F_{CO_2}$  and  $K_{CO_2}$ . Using the value of  $K_{CO_2} = 60$ , interpolated for CO<sub>2</sub> at 800 °C, with the approximate from  $[P_{CO_2}]_{10:90} / [P_{CO_2}]_{pure} \sim 1.5$  from Figure 2, we

$$\text{see } \frac{[1 + \frac{F_{CO_2}(60)}{1 + 0.0854(10) + 0.0261(90)}]}{[1 + \frac{F_{CO_2}(60)}{1 + 0.0854(100)}]} = 1.5. \text{ Clearly, my colleague, Nicholas Leon can compare this}$$

estimation to what he finds in his detailed work for pure CO<sub>2</sub> vs. 10% CO<sub>2</sub> with a 10:90 feed at 100 psia for his CMS created by pyrolysis at 800C like used by Zhang in Figure 2.

An additional discussion item relates to results reported by Zhang pore size evolution apparent in Figure 9a-e. I think my results for  $C'_{L,CH_4}$  and  $C'_{L,CO_2}$  may be consistent with this trend. Specifically, emergence of small peaks for pyrolysis for 750 °C → 900 °C in Figure 9a-e may suggest changes in micropore wall morphology enabling access to CO<sub>2</sub> but possibly not CH<sub>4</sub>. Although speculative, if ultramicropores in the walls indicated by this emergent capacity exclude CH<sub>4</sub>, it would provide direct information supporting the basis for the exclusion selectivity in favor of CO<sub>2</sub> vs. CH<sub>4</sub>. This result can also clearly help explain exclusion selectivity for the additional important H<sub>2</sub>/CH<sub>4</sub> pair, that is starting to be pursued by other colleagues in the Koros group that shows even higher permselectivity of 40,000 vs. that of “only” 3500 for CO<sub>2</sub>/CH<sub>4</sub> studied in this thesis. Such ultraselectivity for H<sub>2</sub>/CH<sub>4</sub> is especially exciting since it addresses renewed interest in H<sub>2</sub> as a carbon-free energy carrier. Specifically, CMS separation modules with ultrahigh selectivities for H<sub>2</sub>/CH<sub>4</sub> may provide the basis for hydrogen extraction modules (HEMs). Such HEMs could enable using the huge natural gas pipeline network as a hybrid carrier in which HEMs allow high purity H<sub>2</sub> extraction at points of use for fuel cells or hydrogen refueling stations or other direct uses (3-4).

## 5.6 References

1. Kiyono, M; Koros, WJ; Williams, PJ, Chapter 7, “Correlation between pyrolysis atmosphere and carbon molecular sieve membrane performance properties,” in *Correlations in Membrane Science*, Ed. by S. T. Oyama and S. S. Williams, Elsevier Science Publishers, *Advances in Membrane Science Series*, p. 137-171 (2011).
2. Zhang, C; Koros, WJ, Ultraselective Carbon Molecular Sieve Membranes with Tailored Synergistic Sorption Selective Properties, *Advanced Materials*, 29 (33), Article Number: 1701631(2017).
3. <https://www.energy.gov/eere/fuelcells/articles/hyblend-technical-summary>.
4. B. Zornoza, C. Casado and A. Navajas, *Advances in hydrogen separation and purification with membrane technology*, Elsevier, Netherlands (2013).

## CHAPTER 6. CONCLUSIONS AND RECOMMENDATIONS

### 6.1 Conclusions

This thesis makes important contributions to extend work by former group members (1-3) who have shown that a new generation of CMS is emerging. The focus of the work in the current thesis uses the so-called dual mode sorption concept in CMS to understand provocative trends in Zhang's work (2). Moreover, the work provides a foundation for an ambitious PhD project by Nicholas Leon in the Koros group to further extend the dual mode concept beyond the sorption topic studied here. Leon will include diffusion topics involving effects of entropic selectivity that are expected to be reflected in the dual mode model diffusivities and their ratios for CO<sub>2</sub> and CH<sub>4</sub>.

The directly measured sorption coefficients at 35 °C and 100 psia for CO<sub>2</sub> and CH<sub>4</sub> for Matrimid®-derived CMS created for pyrolysis temperatures from 550 °C to 900 °C are consistent with the trends seen based on indirectly measured values by Zhang over the range from 750 °C to 900 °C, validating the typical assumption of local equilibrium in Equations (1-3).

The detailed sorption isotherms for the pure CO<sub>2</sub> and CH<sub>4</sub> at 35 °C for pressures up to 500 psia allowed fitting the dual mode sorption parameters, ( $k_{C,i}$ ,  $C'_{L,i}$ ,  $b$ ,  $K$ ) for both CO<sub>2</sub> and CH<sub>4</sub> using the sorption data in these isotherms. A surprising trend discovered for pyrolysis at 700 °C supports the existence of a maximum in the 100 psia sorption coefficient for CO<sub>2</sub> and CH<sub>4</sub> between 550 and 900 °C pyrolysis suggested by Zhang using his indirect sorption measurements is significant. This maximum suggests that the

vision in Figure 5 of a dual mode environment with tightening Henry's law and Langmuir environments as pyrolysis temperature increases is reasonable.

## 6.2 Recommendations

I recommend the current work extended to include studying sorption isotherms to enable evaluation of enthalpies of sorption from the temperature dependences of the affinity coefficients and Henry's Law coefficients. This was an initial aim of my research, but unfortunately due to time constraints and GEM Fellowship obligations, I was unable to include this feature in this work. Another suggestion is to expand XPS testing on additional samples to document and understand trends in the actual nature of trace elemental amounts at each pyrolysis temperature. This could further support the hypothesis behind why the  $k_{C,i}$  value for CO<sub>2</sub> drops dramatically at higher pyrolysis temperatures versus lower ones if pyrrolic and pyridinic Nitrogen entities are removed. In addition, more pore size analysis similar to that of Dr. Chen Zhang's work discussed in Figure 9a-e should be completed for CMS prepared at lower temperatures below 750 °C and possibly also above 900 °C. Indeed, studying CMS prepared at temperatures above 900 °C for both permeation and sorption should be done to test my hypothesis that selectivity will reach even higher levels with applications across a range of gas pairs.

Although it seems like a minute detail, I also suggest when testing sorption and permeation in a consistent order—and eventually with actual mixed gas feeds. This latter recommendation will not be easily done but will allow testing the mixed gas version of Equation (4) that includes terms related to those in Equation (5) for mixed gas permeation, which is easier to do.

### 6.3 References

1. Kiyono, M; Koros, WJ; Williams, PJ, Chapter 7, “Correlation between pyrolysis atmosphere and carbon molecular sieve membrane performance properties”, in *Correlations in Membrane Science*, Ed. by S. T. Oyama and S. S. Williams, Elsevier Science Publishers, *Advances in Membrane Science Series*, p. 137-171 (2011).
2. Zhang, C; Koros, WJ, Ultraselective Carbon Molecular Sieve Membranes with Tailored Synergistic Sorption Selective Properties, *Advanced Materials*, 29 (33), Article Number: 1701631(2017).
3. Sanyal, O.; Hays, SS; Leon, NE, Guta, YA; Itta, AK; Lively, RP; William J. Koros, A Self-Consistent Model for Sorption and Transport in Polyimide-Derived Carbon Molecular Sieve Gas Separation Membranes, *Angew. Chem. Int. Ed.* 59, 20343 –20347 (2020).

## APPENDIX A. COMPARISON TO PREVIOUS WORK

Conducting these experiments required numerous reconsiderations of previous work by Koros members. One specific member's dissertation that was utilized heavily was that of Dr. Mayumi Kiyono. All films tested in this current thesis were prepared under an inert Argon feed at a rate of 600 standard cubic centimeters (sccm). Due to the work of Kiyono, it was determined that inert gas flow rate does not inhibit or affect film performance in sorption. Initially, after testing many dense films that were prepared under the 600 sccm inert Argon feed, it was believed that inert gas feed amounts could in fact affect its performance in sorption, but it does not. There is no external mass transfer occurring that could explain if that were the case. To prove this, I tested Matrimid® CMS dense film that was prepared to the exact specifications of the film that was tested and discussed by Mayumi. Her film was prepared under 200 sccm Argon feed, and the results that I discovered were nearly identical to hers. The caveat between my depiction and hers, is that she fit her data with a Langmuir isotherm, whereas mine (all seen below) were fitted using the dual-mode model.

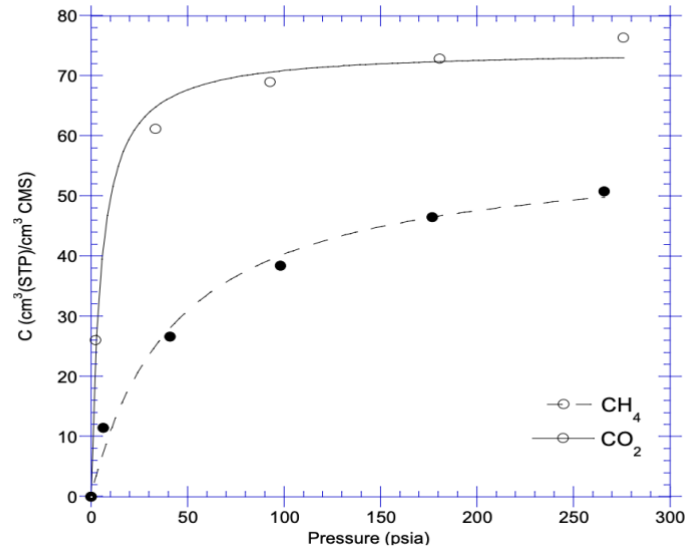


**Figure 17: Kiyono Sorption isotherms for Matrimid® CMS-550 membranes prepared with 1 ppm O<sub>2</sub>/Ar inert pyrolysis. Test temperature was 35°C (1).**

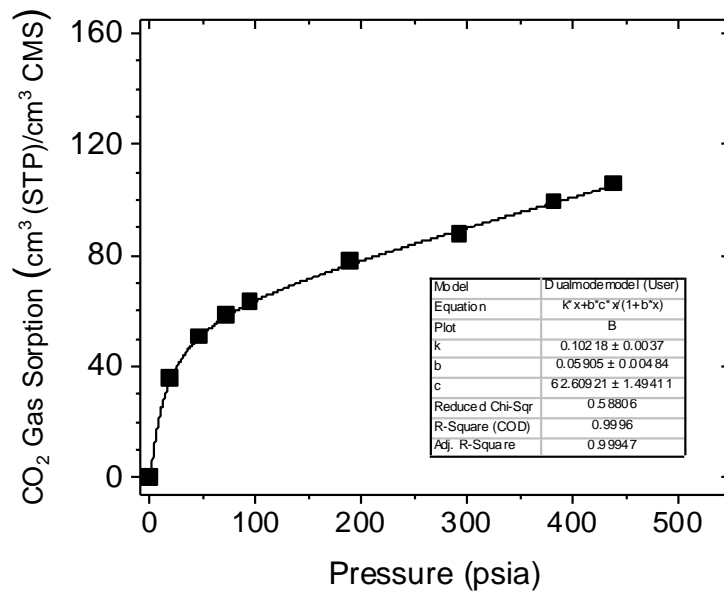


**Figure 18a: Vessel CO<sub>2</sub> Sorption Dual Mode Model fit for Matrimid® CMS-550. Membrane prepared with 1 ppm O<sub>2</sub>/Ar inert pyrolysis. Test temperature was 35 °C.**

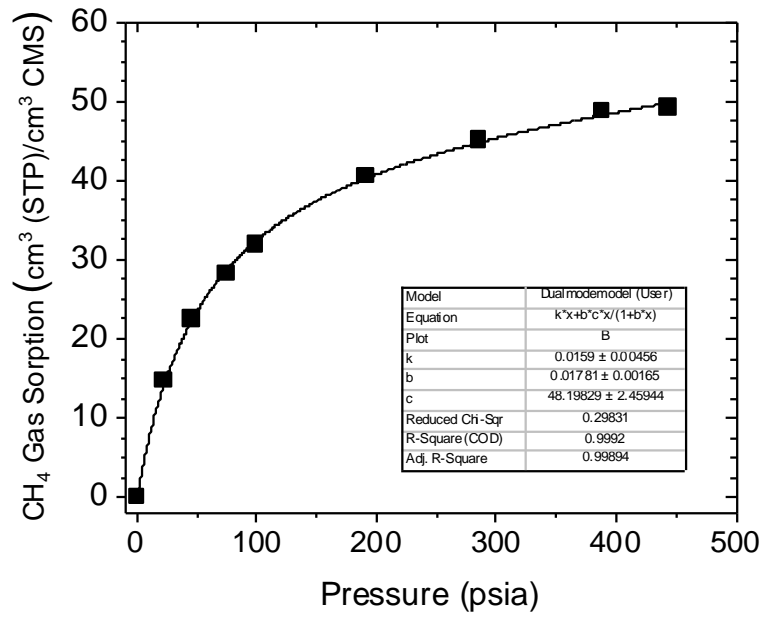


**Figure 18b: Vessel CH<sub>4</sub> Sorption Dual Mode Model fit for Matrimid® CMS-550.**

**Membrane prepared with 1 ppm O<sub>2</sub>/Ar inert pyrolysis. Test temperature was 35°C.**

## **APPENDIX B. ADDITIONAL SORPTION EXPERIMENT DATA**

Appendix B illustrates all data gathered on two different sorption modules in the Koros Group. These two sorption modules had not been recently calibrated. The modules had not been utilized in years due to the COVID-19 pandemic, and therefore the usage of this specific data in this body of work has been excluded. The tables were graciously created by a recent Georgia Tech Bachelor of Science in Chemical Engineering graduate and former member of the Koros Group, Asia Taylor. It is critical to note how important proper calibration is – both volumetric calibration (for the reservoir and cell volumes), as well as transducer calibration.

**Table 8: Matrimid 550C CMS- Methane (CH4)**

Test Number	Test Date	Sorption System	Sorption Temperature (°C)	Pyrolysis Temperature (°C)	Sample Volume (cc)	Aluminum Foil Volume (cc)	Initial Reservoir		Final Reservoir		Initial Reservoir		Final Reservoir		
							Pressure (psi)	Pressure (psi)	Pressure (psi)	Pressure (psi)	Compressibility Factor	Compressibility Factor	Compressibility Factor	Compressibility Factor	
1	2/8/23	Paz	35	550	0.09	0.131	55.406	9.138	103.917	24.756	8.708	0.994	0.999	1.000	0.999
2	2/8/23	Paz	35	550	0.09	0.131	206.274	55.765	206.274	24.756	23.889	0.989	0.997	0.999	0.997
3	2/8/23	Paz	35	550	0.09	0.131	206.274	55.765	206.274	24.756	53.637	0.978	0.994	0.997	0.994
4	2/8/23	Paz	35	550	0.09	0.131	293.656	96.850	293.656	53.633	92.979	0.969	0.990	0.994	0.990
5	2/8/23	Paz	35	550	0.09	0.131	398.559	150.840	398.559	92.988	143.026	0.958	0.984	0.990	0.985
6	2/8/23	Paz	35	550	0.09	0.131	505.802	214.625	505.802	143.028	202.330	0.948	0.977	0.985	0.979
7	2/8/23	Paz	35	550	0.09	0.131	519.507	266.544	519.507	202.324	253.665	0.947	0.972	0.979	0.973

**Table 9: Matrimid 550C CMS- Carbon Dioxide (CO2)**

Test Number	Test Date	Sorption System	Sorption Temperature (°C)	Pyrolysis Temperature (°C)	Sample Volume (cc)	Aluminum Foil Volume (cc)	Initial Reservoir		Final Reservoir		Initial Reservoir		Final Reservoir		
							Pressure (psi)	Pressure (psi)	Pressure (psi)	Pressure (psi)	Compressibility Factor	Compressibility Factor	Compressibility Factor	Compressibility Factor	
1	2/10/23	Paz	35	550	0.09	0.131	65.6168	11.2598	128.5645	31.444	9.7946	0.993	0.998	1	0.999
2	2/10/23	Paz	35	550	0.09	0.131	177.785	57.8762	177.785	29.3293	29.3293	0.9863	0.9966	0.999	0.9969
3	2/10/23	Paz	35	550	0.09	0.131	205.9412	85.052	205.9412	29.33	54.3315	0.9811	0.9938	0.9969	0.9942
4	2/10/23	Paz	35	550	0.09	0.131	294.9873	123.9667	294.9873	54.332	79.777	0.9782	0.9909	0.9942	0.9915
5	2/10/23	Paz	35	550	0.09	0.131	289.6836	151.9967	289.6836	79.7696	116.2244	0.9689	0.9868	0.9915	0.9876
6	2/10/23	Paz	35	550	0.09	0.131	271.2511	153.4569	271.2511	116.2143	144.462	0.9695	0.9838	0.9876	0.9846
7	2/10/23	Paz	35	550	0.09	0.131	271.2511	153.4569	271.2511	144.4375	168.8304	0.9714	0.9837	0.9846	0.9821

**Table 10: Matrimid 550C CMS- Methane (CH4)**

Test Number	Test Date	Sorption System	Sorption Temperature (°C)	Pyrolysis Temperature (°C)	Sample Volume (cc)	Aluminum Foil Volume (cc)	Initial Reservoir Pressure (psi)	Final Reservoir Pressure (psi)	Initial Sample Pressure (psi)	Final Sample Pressure (psi)	Initial Reservoir Compressibility Factor	Final Reservoir Compressibility Factor	Initial Sample Compressibility Factor	Final Sample Compressibility Factor
1	3/1/23	Borges	35	550	0.098	0.119	47,256	8,049	0.006	7,563	0.995	0.999	1.000	0.999
2	3/1/23	Borges	35	550	0.098	0.119	115,410	26,317	7,553	25,222	0.988	0.997	0.999	0.997
3	3/1/23	Borges	35	550	0.098	0.119	244,580	64,190	25,197	61,763	0.974	0.993	0.997	0.993
4	3/1/23	Borges	35	550	0.098	0.119	269,903	91,379	61,775	95,678	0.972	0.990	0.993	0.990
5	3/1/23	Borges	35	550	0.098	0.119	408,183	152,388	95,660	146,266	0.958	0.984	0.990	0.984
6	3/1/23	Borges	35	550	0.098	0.119	515,139	211,668	146,250	205,226	0.947	0.978	0.984	0.978
7	3/1/23	Borges	35	550	0.098	0.119	520,161	262,661	205,223	253,757	0.947	0.972	0.978	0.973

**Table 11: Matrimid 550C CMS- Carbon Dioxide (CO2)**

Test Number	Test Date	Sorption System	Sorption Temperature (°C)	Pyrolysis Temperature (°C)	Sample Volume (cc)	Aluminum Foil Volume (cc)	Initial Reservoir Pressure (psi)	Final Reservoir Pressure (psi)	Initial Sample Pressure (psi)	Final Sample Pressure (psi)	Initial Reservoir Compressibility Factor	Final Reservoir Compressibility Factor	Initial Sample Compressibility Factor	Final Sample Compressibility Factor
1	3/3/23	Borges	35	550	0.098	0.119	65,6168	11,2435	0.041	9,7957	0.993	0.998	1	0.999
2	3/3/23	Borges	35	550	0.098	0.119	128,5645	30,8317	9,7824	29,3258	0.9863	0.9967	0.999	0.9969
3	3/3/23	Borges	35	550	0.098	0.119	177,785	57,8423	29,33	54,328	0.9811	0.9938	0.9969	0.9942
4	3/3/23	Borges	35	550	0.098	0.119	205,9412	85,0583	54,332	79,7758	0.9782	0.9909	0.9942	0.9915
5	3/3/23	Borges	35	550	0.098	0.119	294,9873	125,8844	79,7696	116,2205	0.9689	0.9866	0.9915	0.9876
6	3/3/23	Borges	35	550	0.098	0.119	289,6836	153,8003	116,2143	144,45	0.9695	0.9836	0.9876	0.9846
7	3/3/23	Borges	35	550	0.098	0.119	271,2511	156,3483	144,4375	168,8241	0.9714	0.9834	0.9846	0.9821

Table 12: Matrimid 700C CMS- Methane (CH4)

Test Number	Test Date	Sorption System	Sorption Temperature (°C)	Pyrolysis Temperature (°C)	Sample Volume (cc)	Aluminum Foil Volume (cc)	Initial Reservoir Pressure (psi)	Final Reservoir Pressure (psi)	Initial Sample Pressure (psi)	Final Sample Pressure (psi)	Initial Reservoir Compressibility Factor	Final Reservoir Compressibility Factor	Initial Sample Compressibility Factor	Final Sample Compressibility Factor
1	3/15/23	Paz	35	700	0.097	0.145	71.3917	12.1574	-0.1179	11.3936	0.9924	0.9987	1	0.9988
2	3/15/23	Paz	35	700	0.097	0.145	129.742	31.832	11.2421	30.8642	0.9862	0.9966	0.9988	0.9967
3	3/15/23	Paz	35	700	0.097	0.145	240.9469	68.5384	30.6603	65.6505	0.9745	0.9927	0.9967	0.993
4	3/15/23	Paz	35	700	0.097	0.145	480.058	150.743	65.5076	134.9453	0.9504	0.984	0.993	0.9856
5	3/15/23	Paz	35	700	0.097	0.145	480.0982	220.4305	134.9365	192.0076	0.9503	0.9767	0.9856	0.9796
6	3/15/23	Paz	35	700	0.097	0.145	548.7207	261.2623	175.5202	235.2096	0.9437	0.9724	0.9814	0.9751
7	3/15/23	Paz	35	700	0.097	0.145	546.796	322.5799	218.507	260.406	0.9439	0.9661	0.9769	0.9725

Table 13: Matrimid 700C CMS- Carbon Dioxide (CO2)

Test Number	Test Date	Sorption System	Sorption Temperature (°C)	Pyrolysis Temperature (°C)	Sample Volume (cc)	Aluminum Foil Volume (cc)	Initial Reservoir Pressure (psi)	Final Reservoir Pressure (psi)	Initial Sample Pressure (psi)	Final Sample Pressure (psi)	Initial Reservoir Compressibility Factor	Final Reservoir Compressibility Factor	Initial Sample Compressibility Factor	Final Sample Compressibility Factor
1	3/22/23	Paz	35	700	0.097	0.145	66.1125	11.2402	-0.2035	9.6757	0.9929	0.9988	1	0.999
2	3/22/23	Paz	35	700	0.097	0.145	140.2392	33.0292	9.6353	30.9938	0.9851	0.9965	0.999	0.9967
3	3/22/23	Paz	35	700	0.097	0.145	228.3354	68.797	31.0095	64.206	0.9758	0.9926	0.9967	0.9931
4	3/22/23	Paz	35	700	0.097	0.145	228.5675	97.7571	64.2091	91.2953	0.9758	0.9896	0.9931	0.9903
5	3/22/23	Paz	35	700	0.097	0.145	219.2325	118.0401	91.3059	112.0495	0.9768	0.9874	0.9903	0.9881
6	3/22/23	Paz	35	700	0.097	0.145	224.0437	136.2362	112.0439	129.9619	0.9763	0.9855	0.9881	0.9862

**Table 14: Matrimid 900C CMS- Methane (CH4)**

Test Number	Test Date	Sorption System	Sorption Temperature (°C)	Pyrolysis Temperature (°C)	Sample Volume (cc)	Aluminum Foil Volume (cc)	Initial Reservoir Pressure (psi)	Final Reservoir Pressure (psi)	Initial Sample Pressure (psi)	Final Sample Pressure (psi)	Initial Reservoir Compressibility Factor	Final Reservoir Compressibility Factor	Initial Sample Compressibility Factor	Final Sample Compressibility Factor
1	4/4/23	Paz	35	900	0.097	0.145	78.2814	12.9946	0.0083	12.905	0.9916	0.9986	1	0.9986
2	4/4/23	Paz	35	900	0.097	0.145	145.2904	35.222	12.7599	34.6442	0.9845	0.9962	0.9986	0.9963
3	4/4/23	Paz	35	900	0.097	0.145	305.5428	82.4923	34.625	79.6447	0.9679	0.9912	0.9963	0.9915
4	4/4/23	Paz	35	900	0.097	0.145	480.3794	153.9196	79.2244	146.1186	0.9503	0.9836	0.9915	0.9845
5	4/4/23	Paz	35	900	0.097	0.145	530.6591	222.1797	146.0842	209.1352	0.9454	0.9765	0.9845	0.9778
6	4/4/23	Paz	35	900	0.097	0.145	549.3779	276.7352	207.4731	263.0644	0.9436	0.9708	0.978	0.9722
7	4/4/23	Paz	35	900	0.097	0.145	581.4535	329.7257	262.9998	314.1834	0.9406	0.9654	0.9722	0.967
8	4/4/23	Paz	35	900	0.097	0.145	579.297	371.141	314.0155	356.1178	0.9408	0.9612	0.967	0.9627
9	4/4/23	Paz	35	900	0.097	0.145	597.8837	409.2029	355.9597	394.0214	0.939	0.9574	0.9627	0.9589
10	4/4/23	Paz	35	900	0.097	0.145	616.8474	443.8404	393.9115	428.7319	0.9373	0.9539	0.9589	0.9554
11	4/4/23	Paz	35	900	0.097	0.145	616.4588	471.678	428.5717	457.595	0.9373	0.9512	0.9554	0.9526
12	3/22/23	Paz	35	700	0.097	0.145	589.0936	488.3487	457.5505	477.6113	0.9399	0.9495	0.9526	0.9506
13	3/22/23	Paz	35	700	0.097	0.145	569.2878	499.8531	477.5653	491.3621	0.9417	0.9484	0.9506	0.9492

**Table 15: Matrimid 900C CMS- Carbon Dioxide (CO2)**

Test Number	Test Date	Sorption System	Sorption Temperature (°C)	Pyrolysis Temperature (°C)	Sample Volume (cc)	Aluminum Foil Volume (cc)	Initial Reservoir Pressure (psi)	Final Reservoir Pressure (psi)	Initial Sample Pressure (psi)	Final Sample Pressure (psi)	Initial Reservoir Compressibility Factor	Final Reservoir Compressibility Factor	Initial Sample Compressibility Factor	Final Sample Compressibility Factor
1	4/6/23	Paz	35	900	0.097	0.145	155.9855	27.5356	0.0052	25.4677	0.9834	0.9971	1	0.9973
2	4/6/23	Paz	35	900	0.097	0.145	228.9561	63.6822	25.3614	59.7626	0.9758	0.9932	0.9973	0.9936
3	4/6/23	Paz	35	900	0.097	0.145	227.5263	93.1383	59.9832	87.7581	0.9759	0.9901	0.9936	0.9906
4	4/6/23	Paz	35	900	0.097	0.145	218.8483	114.6858	87.7616	109.1415	0.9768	0.9878	0.9906	0.9884
5	4/6/23	Paz	35	900	0.097	0.145	230.6782	134.9077	105.1865	128.8117	0.9756	0.9856	0.9884	0.9863
6	4/6/23	Paz	35	900	0.097	0.145	324.1431	172.5233	128.8099	160.9992	0.966	0.9817	0.9863	0.9829
7	4/6/23	Paz	35	900	0.097	0.145	450.4148	227.9162	160.9924	210.6337	0.9533	0.9759	0.9829	0.9777
8	4/6/23	Paz	35	900	0.097	0.145	585.7173	364.148	283.6361	335.1097	0.9402	0.9619	0.9701	0.9648
9	4/6/23	Paz	35	900	0.097	0.145	589.1565	407.0909	335.0832	377.016	0.9399	0.9576	0.9648	0.9606
10	4/6/23	Paz	35	900	0.097	0.145	623.0875	452.1617	376.9752	417.3475	0.9367	0.9531	0.9606	0.9565
11	4/6/23	Paz	35	900	0.097	0.145	621.3288	480.4207	417.2455	449.6525	0.9368	0.9503	0.9566	0.9533